Quaternary Science Reviews
July 2023, Volume 311 Pages 108145 (24p.)
https://doi.org/10.1016/j.quascirev.2023.108145
https://archimer.ifremer.fr/doc/00841/95248/

Palynology, palaeoclimate and chronology from the Saalian Glacial to Saint-Germain II interstadial from two long cores at the limit between the Mediterranean and Euxinian regions

Leroy S.A.G. [1, 2, 3, *], Henry P. [1], Peyron O. [4], Rostek F. [1], Kende J. [1], Bard E. [1], Tachikawa K. [1]

[1] Aix Marseille Univ, CNRS, IRD, INRAE, Coll France, CEREGE, Aix-en-Provence, France
[2] Aix Marseille Univ, CNRS, Minist. Culture & Com., LAMPEA, 13094 Aix-en-Provence, France
[3] School of Environmental Sciences, University of Liverpool, L69 3GP Liverpool, UK
[4] Institut des Sciences de l'Evolution de Montpellier, ISEM, CNRS, IRD, EPHE, Université de Montpellier, Montpellier, France

* Corresponding author : S. A. G. Leroy, email address : suzleroy@hotmail.com

henry@cerege.fr ; odile.peyron@umontpellier.fr ; rostek@cerege.fr ; jj.kende@gmail.com ; bard@cerege.fr ; tachikawa@cerege.fr

Abstract :

The Marmara region (NW Turkey) has a transitional vegetation and climate between the Mediterranean one and the Euxinian one. For the last Interglacial period or Eemian and following the two Saint-Germain Interstadials (i.e. c. MIS 5), as well and the previous glacial, the Saalian, no vegetation or climate information is available yet. Here we provide the results of the pollen analysis of two sediment cores taken from the Sea of Marmara. We focus on the period below a major erosion horizon, i.e. the red-H1 seismic horizon, which corresponds to the last Interglacial and a large part of the previous glacial period. A palaeoclimatic reconstruction inferred from pollen assemblages is also proposed here.

Based on geochemistry that allows inter-core comparison and on a succession of warm and cold phases derived by pollen analysis, a nearly complete sequence from the Saalian Glacial period (c. MIS 6) to the Saint-Germain II Interstadial (MIS 5a) was obtained, despite the occurrence of hiatuses corresponding often to lowstands.

The Pterocarya extinction has been traced from MIS 7 in Italy to Saint-Germain I Interstadial (c. MIS 5c) in the eastern Sea of Marmara, showing a progressive retreat from west to east until the Black Sea region, where it is still present nowadays.

The climatic changes reconstructed for the Eemian Interglacial (or c. MIS 5e) are characterised by warmer temperature and a slightly drier climate than at present, at its peak. This pattern is in agreement with the Ohrid climate pattern, in the Balkans. In the Marmara region, this is reflecting a shift of the Mediterranean climate towards the NE and a reduction of the Euxinian vegetation.

Highlights

► Pollen analyses of last Interglacial and previous Glacial in Sea of Marmara. ► Progressive *Pterocarya* extinction from MIS7 in S. Europe to MIS5c in Sea of Marmara. ► Reduction of Euxinian vegetation and extension of the Mediterranean one during Eemian. ► Eemian warmer and slightly drier than present climate.

Keywords : Eemian interglacial, Saalian glacial, Pollen-inferred palaeoclimatic reconstruction, Euxinian vegetation, Marmara sea, Pterocarya

1 Introduction

The warmest part of the last interglacial, called the Eemian Interglacial from 130 to 110 ka, corresponding roughly to Marine Isotopic Stage 5e (MIS 5e) (Shackleton et al., 2003), is a key period for obtaining an insight of our future, as the sea levels and temperatures were higher than the present. A sea-level rise of 6 to 7 m was estimated, in comparison to today, at 127 ka ago in the West Mediterranean Sea (Poliak et al., 2018). The air temperature of the Eemian Interglacial in the central/eastern Mediterranean region has been reconstructed from proxy records and model outputs: temperature was estimated to be ca. 2 ºC warmer than today leading to significant vegetation zone shifts (Brewer et al., 2008; Fischer et al., 2018; On and Özeren, 2019; Sinopoli et al., 2019). The last Interglacial period, and in particular the Eemian (or c. MIS 5e), offers a testbed for comparing climatic change throughout an interglacial with the current warm period and its near future. Here results from climatic reconstructions from two pollen records distributed across the Sea of Marmara (Turkey) are presented, allowing an assessment of trends and regional averages of climatic changes during this period.

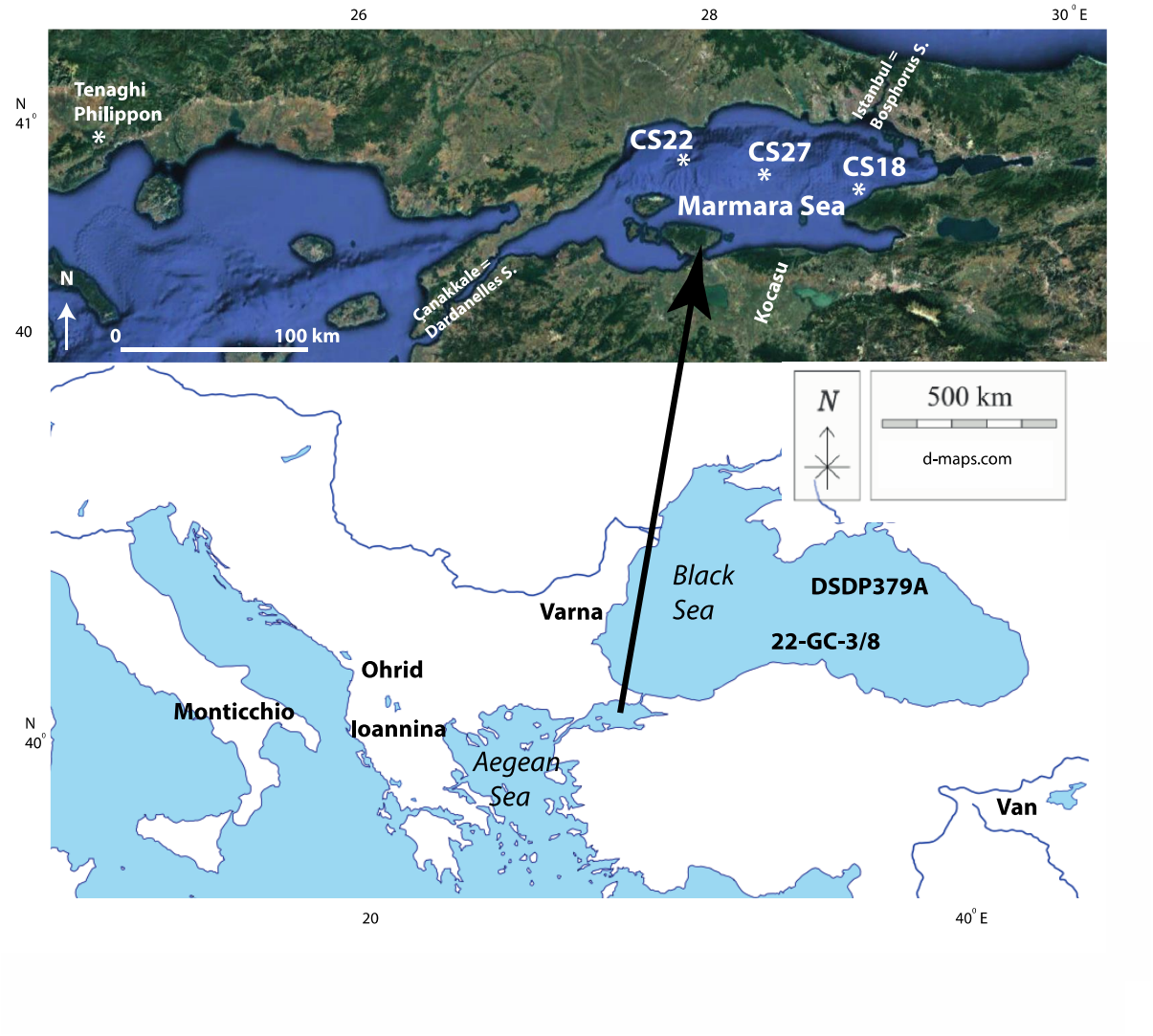

Figure 1: Top: Map of the region around the Marmara Sea with the two studied cores CS22 and CS18 and additional information from core CS27, and the pollen site of Tenaghi Philippon. Bottom: location of the Marmara Sea in the Ponto-Caspian region with some other pollen sequences used for comparison.

In the Eastern Mediterranean region, the area around the Sea of Marmara (SoM) is environmentally sensitive. It is intermediate between the Mediterranean and temperate ecosystems as shown by a 23 ka-long record of vegetation from the Western High in the Marmara Sea (Valsecchi et al., 2012). This meeting point

between Europe and Asia is also one of the main migration routes of humans from Africa to Europe (Leroy et al., 2011; Müller et al., 2011; Nielsen et al., 2017). Vegetation and climatic changes during the Eemian are poorly investigated in the Marmara region as long sequences are so far lacking (Felde et al., 2020). The nearest vegetation reconstruction covering the last interglacial is in Tenaghi Philippon, a key site in Greece, 370 km to the west (Wijmstra and Smit, 1976; Milner et al., 2013; 2016) (Fig. 1). Further afield to the west are the sites of Ioannina in Greece (Tzedakis et al., 2002), Monticchio in Italy (Brauer et al., 2007), Lake Ohrid at the border between Macedonia and Albania (Balkan Peninsula), the oldest extant lake in Europe (e.g. Lézine et al., 2010; Sadori et al., 2016; Holtvoeth et al., 2017; Sinopoli et al., 2019; Wagner et al., 2019; Donders et al., 2021), and further away to the east of Turkey, Lake Van (Pickarski et al., 2015; 2017) (Fig. 1). For a vegetation type (i.e. Euxinian) similar to that of the SoM, two pollen records are available, but both rather short and at great distances (>500 km). Firstly, a pollen record at the northern limit of the Euxinian vegetation, from the Bulgarian coast near Varna covers the Eemian Interglacial per se, MIS5e (Bozilova and Djankova, 1976) (Fig. 1). Secondly, vegetation reconstructions reflecting northern Anatolia during part of the last interglacial are also available from the S-E Black Sea in core 22-GC3/8 (134-119 ka, Shumilovskikh et al., 2013) (Fig. 1). In addition, in core DSDP 42B, hole 379A in the central-east Black Sea, a pollen record possibly covers the whole Karangatian or MIS 5 but the diagram has a very low sampling resolution and the sequence has no absolute chronology (Koreneva and Kartashova, 1978) (Fig. 1).

Similarly to vegetation changes, climatic changes are also poorly documented in the Marmara region. Reconstruction of palaeoclimatic changes in the SoM region are not available. Some of the Italian and Balkans records (Monticchio and Ohrid

sequences) have been used to reconstruct quantitatively climatic changes during the Eemian based on pollen data (Brewer et al., 2008; Allen and Huntley, 2009; Sinopoli et al., 2019) or on molecular biomarkers proxy (Holtvoeth et al., 2017). These studies indicated different climatic patterns between Europe and the Mediterranean region during the last interglacial, which need to be reinvestigated.

The aims of the current investigation are 1) to establish past vegetation around the SoM, 2) to quantify palaeoclimatic changes during MIS 5 including the stadials and interstadials and 3) to contribute to the age-depth model improvement of the available sequences. Owing to a major European research programme, long sediment cores (up to 30 m) were taken in the SoM during the MARSITE cruise in 2014 to address key questions in earthquake history and palaeoclimates (https://cordis.europa.eu/project/id/308417). In this study, a palaeoclimatic reconstruction around the SoM based on two pollen records obtained from giant piston cores retrieved from the western and eastern parts of the SoM allows us an assessment of trends and regional averages of vegetation and climatic changes during the MIS 6, at 191-130 ka ago and MIS 5 at 130-71 ka ago (Lisiecki and Raymo, 2005) with a special focus on MIS 5e. By tighter inter-core correlations based on new geochemical data, pollen analysis and dinocyst assemblages (the latter detailed in a separate paper: Leroy et al., accepted), by the recognition of the major role plaid by the red-H1 seismic horizon in terms of erosion and by comparing vegetation and climatic reconstruction of the SoM to that of previous obtained on Lake Ohrid sequence, the current study allows building on the previous age hypothesis (Çağatay et al., 2019).

2 Regional setting

The SoM (275 km W-E by 80 km N-S) is located at the western end of the North Anatolian Fault where it splits into several strands along which three deep sub-basins (Tekirdag, Central and Çinarcik) that are separated by two highs: Western and Central Highs (Fig. 1). The deepest part is located in the Çınarcık and Central Basins with approximately 1270 m water depth. In the SE SoM, the Imralı Basin is nowadays a flat area at a water depth only around 300-400 m (Yaltirak, 2002). Rivers are mostly inflowing from the south (Kazancı et al., 2004). The Kocasu (or River Koca) is the main river flowing into the SoM, and it exits now from the continent, south of the Imralı Island. During the lowstand of water level in the SoM, it formed deltas prograding into the Imrali Basin and had largely contributed to filling the shelf of the basin, whereas it incised as submerged canyon during the last glaciation, today providing sediment to the Çınarcık Basin (Kazancı et al., 2004; Sorlien et al., 2012) (Fig. 1). The region immediately around the SoM is relatively flat, although slightly further afield mountains up to 2500 m are found in the S and SE and 1000 m in the N.

A statistical analysis of the current climate at the scale of Turkey shows that the SoM falls at the limit between two very similar clusters: the Marmara cluster, that includes the south-western most part of the Black Sea (mean temperature of 13.7 ºC and mean annual precipitation of 686 mm) and the Aegean-West Mediterranean cluster (with a slightly higher mean temperature of 15.4 ºC and a quasi-identical mean annual precipitation of 682 mm) (Unal et al., 2003). The Black Sea region in their study has an identical temperature to the Marmara region, but nearly twice its precipitation (1176 mm). Precipitation falls primarily in winter and originates mostly from the Westerlies. In addition, across the year, some influence from the Black Sea

may be felt in the SoM. Clearly the Marmara region is a zone of strong longitudinal gradient. Indeed, at the season level, it is located in an area with a strong summer drought gradient between one of the driest regions of Turkey, i.e. the Aegean-Mediterranean region and the wettest one, i.e. the Black Sea coast (Kutiel and Türkeş, 2017).

The potential vegetation in the area is the Euxinian forest, near the limits of the Mediterranean woodland climax (Beug, 1967; Zohary, 1973). The Euxinian forest is characterised by the relic nature of many mesophilous trees and shrubs, such as *Pterocarya fraxinifolia* (Browicz, 1989). According to Atalay and Efe (2010), the SoM is surrounded by sub-humid forests of *Quercus* and *Pinus nigra*. In addition, in the drier south, forests of *Pinus brutia* are frequent. On the north-facing mountain slopes sub-humid to humid forests of *Abies, Fagus* and *P. nigra* occur. In the drier extreme west that has a clear Mediterranean character, pure *P. brutia* forests are common; they may be replaced by macchia when they are degraded. Broad-leaved humid forests (*Fagus, Tilia, Castanea* and *Carpinus betulus*) are only present the E and NE of the SoM on the Black Sea coast. The westernmost distribution of *Pterocarya fraxinifolia* currently just touches the Gulf of Izmit in the eastern Marmara (Browicz and Zielinski, 1982).

3 Previous investigations on cores CS22, CS27 and CS18 in the Marmara Sea

Our study focuses on vegetation and climate changes provided by cores CS22 and CS18 in the SoM, with some supporting information from core CS27. The main lithological and textural variations together with geochemical properties of the

cores were previously published (Kende, 2018; Çağatay et al., 2019), thus, they are not described again here.

3.1 Cores and sedimentological and geochemical methods

The three calypso cores (piston) were taken by the vessel “Pourquoi Pas?” in 2014. Core **CS22** (20.42 m long) was obtained close to the top of the Western High at 40,83 latitude N, 27,79 longitude E and 551 m water depth. On the western edge of the Imralı Basin, core **CS27** was taken at 40,79 N, 28,87 E, by 313 m bsl, and is 20.45 m long. Core **CS18** (14.05 m long) was acquired from a slope of the north-eastern Imralı Basin at 40,66 latitude N and 28,87 longitude E by 291 m water depth (Fig. 1). Visual core descriptions and photographic records were kept for each core.

Total Organic Carbon (TOC) of core CS22 was measured with a gas chromatographic elemental analyzer (Fisons NA1500) on freeze-dried material (Kende, 2018). For cores CS18 and CS27, TOC analysis was obtained at 5 cm interval but increased to a resolution of 2.5 cm in some parts of the sapropels (Çağatay et al., 2019). The TOC content in freeze-dried samples was analysed using a Shimadzu TOC/TIC analyser.

For bulk density from gamma-ray absorption, core CS22 was run through a GEOTEK Multi-Sensor Core Logger (MSCL) before splitting. Analyses were obtained at a 1 cm step (Kende, 2018). For cores CS18 and CS27, gamma density was measured at 2 cm resolution, also using a GEOTEK MSCL (Çağatay et al., 2019).

In core CS22, bulk sediment Ca relative abundance was obtained from an ITRAX core scanner (COX, analytical Systems) for conducting X-ray fluorescence (XRF) analysis at 5 mm resolution, using a Mo tube at 30 kV, 45 mA and 15 s counting time (Kende, 2018). A resolution of 0.5 mm was reached in the laminated sediment. Cores CS18 and CS27 were analysed for multi-element composition at

0.5 mm resolution using an ITRAX µ-XRF core scanner, equipped with XRF-EDS (Çağatay et al., 2019). A fine-focus Mo X-ray tube was used as the source.

3.2 Previous results

The investigations of Kende (2018) and Çağatay et al. (2019) showed us a sedimentary record with three sapropels and, despite some hiatuses, covering the time period since MIS 6 based on ^{14}C age-depth models of the core together with tephra and sapropel layers and a correlation of the Ca XRF intensities with the NGRIP $\delta^{18}O$ record.

The high reflectivity and negative polarity of the red-H1 reflector in high-resolution seismic profiles is probably caused by the contrast of density between high porosity organic-rich sediment in the sapropel layers below and lacustrine sediment above (Kende, 2018). In addition, a graded sand layer of at least a one centimetre thickness is found at the base of the lacustrine section (MIS 4 to 2) in all cores and enhances the reflectivity of the horizon on chirp profiles. The eroded (or non-depositional) interval appears to vary laterally in seismic profiles and notably in some IFREMER 3D box, where it also appears that sedimentations could have remained continuous in ponded basins (Grall et al., 2014). In the Imrali Basin, it may be noted that in core CS20, which is only 1 km from CS27 but on the uplifted side of a fault scarp, the red-H1 horizon is at about 8 m depth, the sapropel layer below is only 30 cm thick, and the Eemian is apparently only recognizable as a couple of foraminifer-bearing sand layers. Overall, it is a reflector found widely across most of the SoM (e.g. Okay et al., 2022). It is a major erosion horizon at the seismic scale, much larger than other erosion levels identified further down the cores, and thus probably much longer. The red-H1 seismic reflector is suggested to be close to the limit between MIS 5 and 4. At least on slopes and topographic highs, it reflects a

hiatus caused by mass-wasting and erosion related to sea-level lowering (Grall et al., 2014; Çağatay et al., 2019). In core CS18, the hiatus caused by this erosion is considered to include the MIS 5 - MIS 4 transition, and to run from 79.3 to 70.1 ka BP (Çağatay et al., 2019). The current investigation focusses on the sediment below the red-H1 reflector.

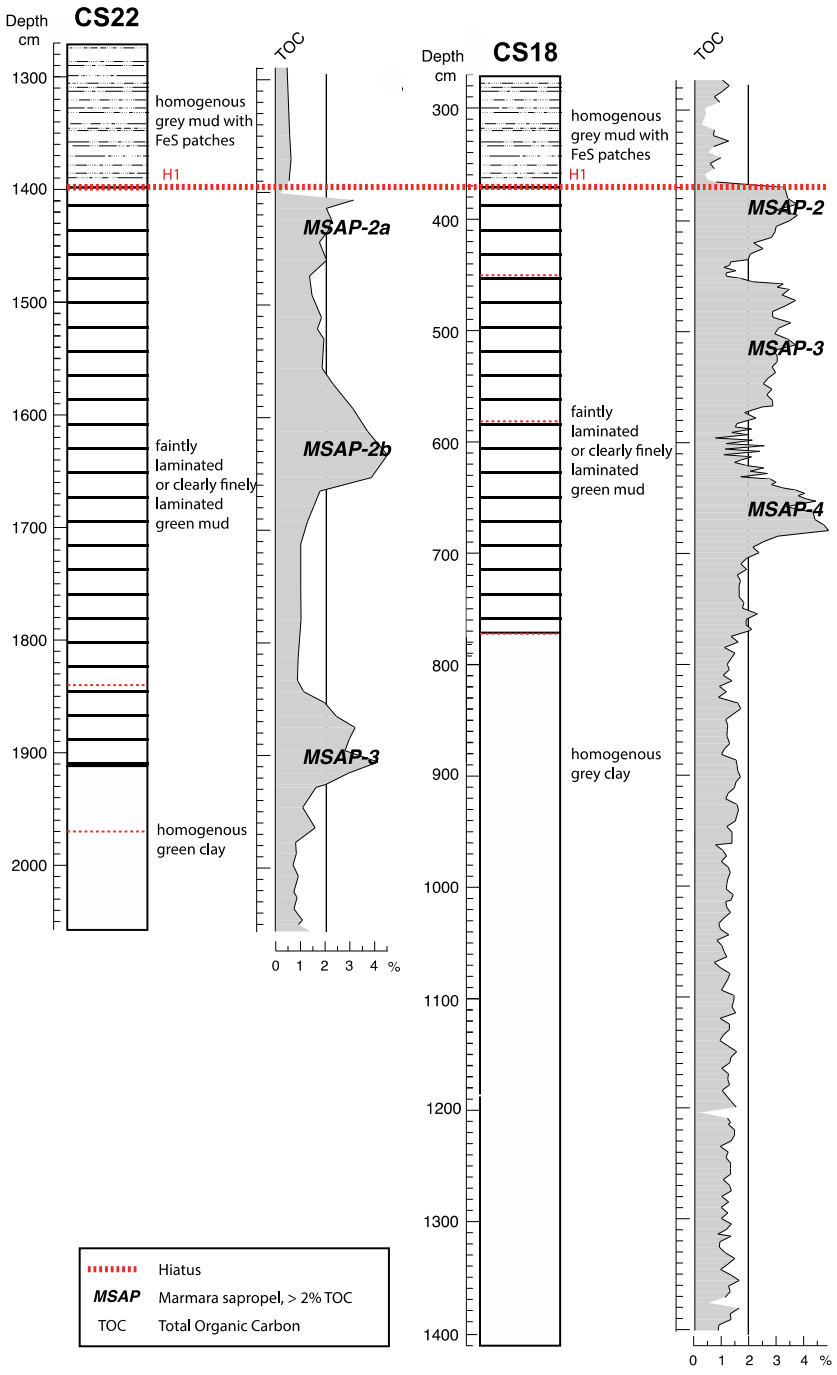

Figure 2: Logs of cores CS22 and CS18 and organic matter percentages (TOC%). Red lines for coarser layers.

Detailed lithological descriptions can be found for cores CS22, CS27 and CS18 in Kende (2018) and Çağatay et al. (2019). Briefly, the sediment is a grey or green clay to silty clay at times clearly finely laminated (Fig. 2). Three sapropels (darker and finely laminated sediment rich in organic matter, >2 % TOC) were tentatively attributed to MIS 5e, 5c and 5a based on correlation of the Ca XRF intensity with the NGRIP $\delta^{18}O$. These are for core CS22, Marmara sapropel 3 (MSAP-3) at 1920-1853 cm and MSAP-2 in two parts: MSAP-2b at 1653-1570 cm and to a lesser extent MSAP-2a at 1460-1407 cm (their naming is adapted from Çağatay et al. (2009)); and for core CS18: MSAP-4 at 699-623 cm, MSAP-3 at 568-455 cm and MSAP-2 at 430-370 cm depth. In core CS27, MSAP 2 and MSAP-3 were identified (Fig. 3).

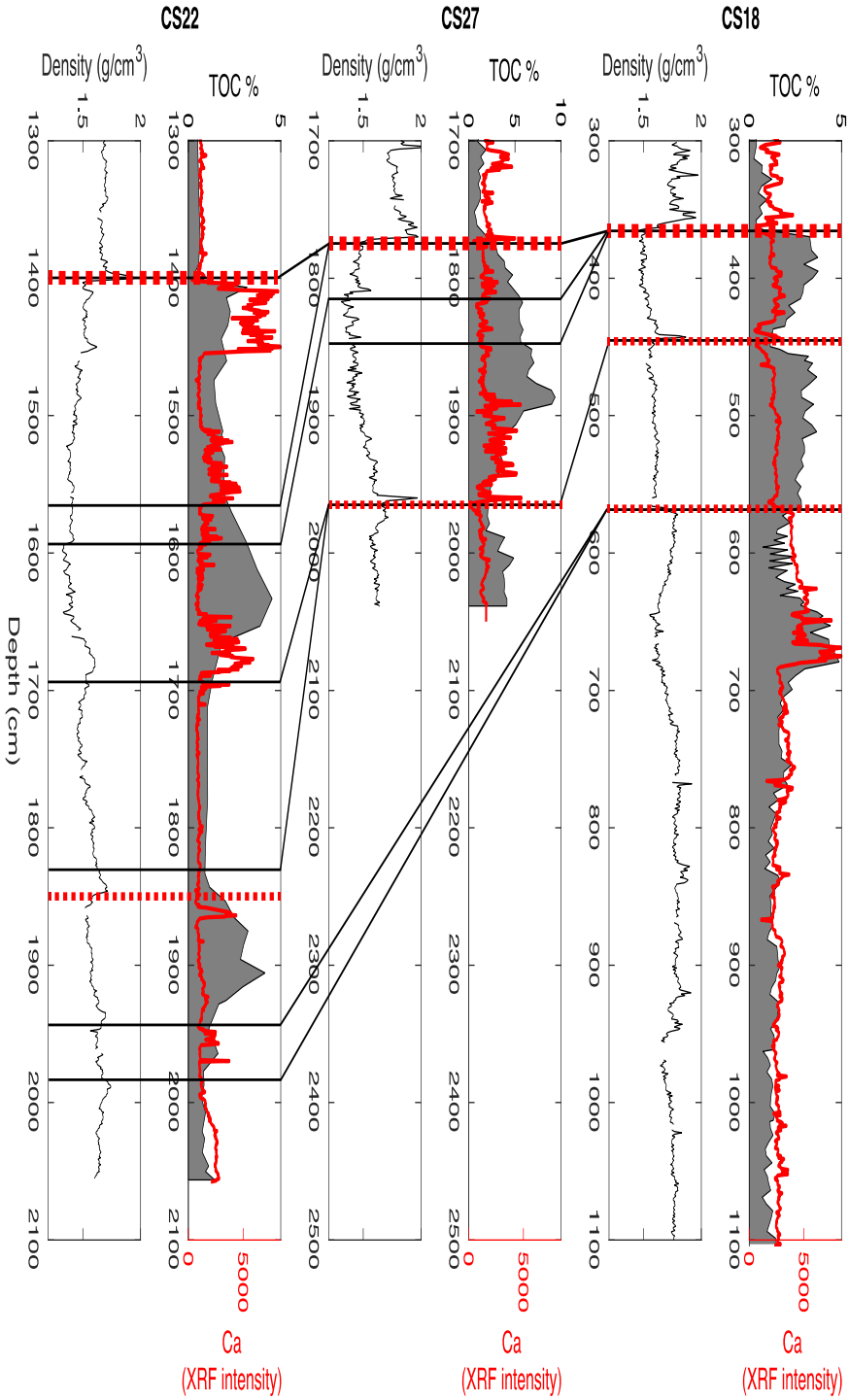
CS22
CS27
CS18
Density (g/cm3)
TOC %
Depth (cm)
Ca
(XRF intensity)

Figure 3: Correlation between cores CS22, CS27 and CS28 based on Ca XRF intensity geochemistry. Black lines: time/depth correlation. Red lines: hiatus correlation (thicker for the red-H1 seismic reflector).

Some coarser layers are found as follows (Fig. 2 and 3). In core CS22, a well-sorted 3 cm-thick sand layer at 1402-1399 cm (correlated with the red-H1 seismic reflector), two centimetric silt layers at 1845 and 1842 cm and centimetric sand lens at 1970 cm have been observed. The sediment below 1970 cm contains many minor normal or listric microfaults and bioturbated silt patches. This indicates that movements along the slope occurred before or around the time of their deposition.

In core CS18, a 1.5 cm-thick coarse silt layer rich in shell debris that has been correlated to the red-H1 reflector layer at 369 cm, a 1 cm-thick fine sand layer at 451 cm, a 1 cm-thick sand layer with shell debris at 580 cm depth and a 0.2 cm-thick silt layer at 772 cm depth are noted. Overall, the silty-sandy layers are thicker and coarser than in core CS22. Two rounded pebbles were found at 759 and 775 cm depth. Thus not only the red-H1 reflector represents an episode of erosion (and hiati), but presumably the sand layers below too. Moreover, core CS18 was taken on a slope where some erosion along shallow gullies is occurring in the Holocene (Henry and Kende, 2015) and thus may be expected to have also occurred in the past. Indeed, the sand layer at 580 cm is associated with a density and porosity contrast between muddy sediment above and below that indicates a discontinuity in the sedimentation process.

Two coarser layers are observed in core CS27 (Fig. 3). The red-H1 reflector at 1783 cm is characterised by a 3 cm-thick well-sorted medium to fine grade sand

layer with an erosional basal contact. An additional horizon, i.e. a 4.5 cm graded sand to silt around 1975 cm depth, also has an erosional base.

In previous studies (Kende, 2018 and Çağatay et al., 2019), in the absence of absolute ages and tephras, the chronology below MIS 3 and especially below the red-H1 seismic reflector, remained tentative. The investigations of Kende (2018) proposed two age-depth models with the base of core CS22 either at the end of MIS 5e or 5a according to the recognition of a major hiatus at 14 m or not respectively. In a following-up and more developed multidisciplinary paper by Çağatay et al. (2019), three cores, i.e. CS18, CS27 and CS22, were correlated to each other using density or Ca peaks. The chronology of two of these cores was supported by a comparison of the Ca curve with NGRIP oxygen isotope record. In addition, it was postulated that sapropels formed during the last interglacial and the two subsequent interstadials (i.e. MIS 5a, c and e) and under anoxic and marine conditions and that the in-between periods, i.e. the stadials MIS 5b and d, were deposited in lacustrine or in low TOC marine conditions (< 2%) (Çağatay et al., 2019). In the same paper, the bottom water conditions were mainly identified by a qualitative study of biota in the sand fraction. The sapropel occurrence was mainly determined visually for core CS22 and both visually and by TOC analysis in core CS18. A nearly complete MIS 5 was then suggested in core CS22 (MIS 5d to 5a) and a complete MIS 5 in core CS18. This is now partially revised.

4 Material and methods

4.1 Pollen and non-pollen palynomorph analysis

Pollen analysis in marine sediment is a valid method to reconstruct past vegetation, as shown by studies linking pollen analysis in surface samples and

adjacent vegetation belts, e.g. for the South China Sea see Sun et al. (1999) and for NW Africa see Hooghiemstra et al. (2006). Pollen falling on the water surface is rapidly eaten by zooplankton and then by fish. It falls then nearly vertically as faecal pellets to the sea bottom. The SoM, due to the relatively short distance between the source and the sink of pollen and due to relatively small water depths, behaves in between a lake and a sea, both in its marine and lake phases. Biomisation in the Ponto-Caspian region, on a mix of modern sediment samples including marine ones, has proved to be a valuable tool to reconstruct past vegetation (Marinova et al., 2017). Additionally in many cases, marine palynology involves the study of non-pollen palynomorphs and organic-walled dinoflagellate cysts found in the same slides (for the Ponto-Caspian: Mudie et al., 2011; Leroy et al., 2014). The latter microfossils provide information on water conditions, thus dramatically expanding information by bridging terrestrial and aquatic domains.

Fifty-one samples were treated in core CS22 and 79 in core CS18 mostly below the red-H1 reflector. The sampling resolution varied between 10 and 20 cm. After measurement of the volume (between 0.5 and 2.5 ml), one tablet of *Lycopodium* was added. The sediment was then soaked in tetrasodium pyrophosphate, followed by acid attacks: cold HCl, cold HF and again cold HCl. Then the samples were rinsed with water and sieved on disposable nylon meshes of 125 and 10 µm. The residues were transferred to vials and slides mounted in glycerol. At least 300 terrestrial pollen grains were counted in each sample, and at least 120 terrestrial pollen grains outside *Pinus*. Some gritty samples in core CS18 were also centrifuged in Sodium Polytungstate at a density of 2.4. All samples (except one at 364 cm depth in core CS18) were rich in palynomorphs. All percentages are obtained on the sum of terrestrial pollen. Concentration in

palynomorphs is calculated in ml of wet sediment. Zonation (on 20 and 24 terrestrial taxa respectively in cores CS22 and 18) was made by CONISS (after square-root transformation), available in the psimpoll software (Bennett, 2007), which was also used for plotting palynological diagrams.

Identifications of pollen were made with the support of the atlas of Reille (1992, 1995 and 1998) and Beug (2004). Non-pollen palynomorphs (NPP) were identified with the help of the plates found in van Geel and Aptroot (2006) and Mudie et al. (2011) amongst many others. Incertae Sedis 5b (probably a green alga) was illustrated in Leroy (2010) for Caspian Sea sites.

The dinoflagellate cysts were counted as well and are the topic of a separate paper. In supplementary information SI1, dinocyst taxon lists with general affinities (brackish, marine, seasonal contrast indicators, warm-loving taxa, etc…) are provided. A separate paper deals in details with dinocyst data and their interpretation (Leroy et al., accepted).

4.2 Palaeoclimatic reconstruction

To reconstruct climatic parameters from pollen data, available methods have their own set of advantages and limitations (e.g. Chevalier et al., 2020) and the selection of the most appropriate technique to be used on fossil pollen record can be complex (Salonen et al., 2019). To estimate climatic changes during MIS 5 from the Marmara pollen sequences, the Modern Analog Technique (MAT; Guiot, 1990) was selected. The MAT is a very sensitive method largely used to provide climatic reconstructions from both terrestrial and marine pollen sequences for different time-periods of the late Quaternary. It has already been tested for the last interglacial, particularly for the Eemian (MIS 5e), and has provided reliable results for this period in Europe (Cheddadi et al., 1998; Brewer et al., 2008; Salonen et al., 2018) and the

Mediterranean area (Sanchez-Goñi et al., 2005; Brewer et al., 2008; Sinopoli et al., 2019). The MAT is an “assemblage approach” in which each fossil pollen sample is compared with a set of modern pollen samples from sites with known environmental/climatic characteristics, relying on a squared log-transferred weighted Euclidean distance measurement. Then modern analogs are selected, from which the (palaeo-) climate parameters are averaged (here four analogues have been selected). As a result, information for temperature and precipitation are yielded.

The modern pollen dataset used here includes 3267 modern pollen samples located in European, Eurasian and Mediterranean areas (Peyron et al., 2013, 2017; Dugerdil et al., 2021). It represents diverse vegetation types and contains many pollen samples from cold and warm steppes and temperate forests. For the MAT, a major limitation can be the occurrence of no-analog situations. For example, during the Eemian, Central European *Carpinus* stands together with *Ilex* occurred (Cheddadi et al., 1998), a floristic composition which generally cannot be found today. Such no-analog situations thus could result in unrealistic reconstruction values. In the Marmara pollen records, the fossil flora is well represented in modern pollen samples; relict taxa are very rare (except samples with taphonomic perturbation, see below). In this frame, the MAT can be applied to the main parts of CS18 and CS22 pollen records. However, samples with taphonomic perturbation (dominance of reworked palynomorphs and fungal spores), must be taken with caution and it was decided to exclude them in the climatic reconstruction.

Five climate parameters were reconstructed, mean annual temperature (TANN), summer precipitations (Psum), mean annual precipitation (PANN), and mean temperature of the coldest /warmest month (MTCO and MTWA). The MAT

method has been applied with the Rioja package from the R environment (Juggins and Juggins, 2019).

5 Palynological results

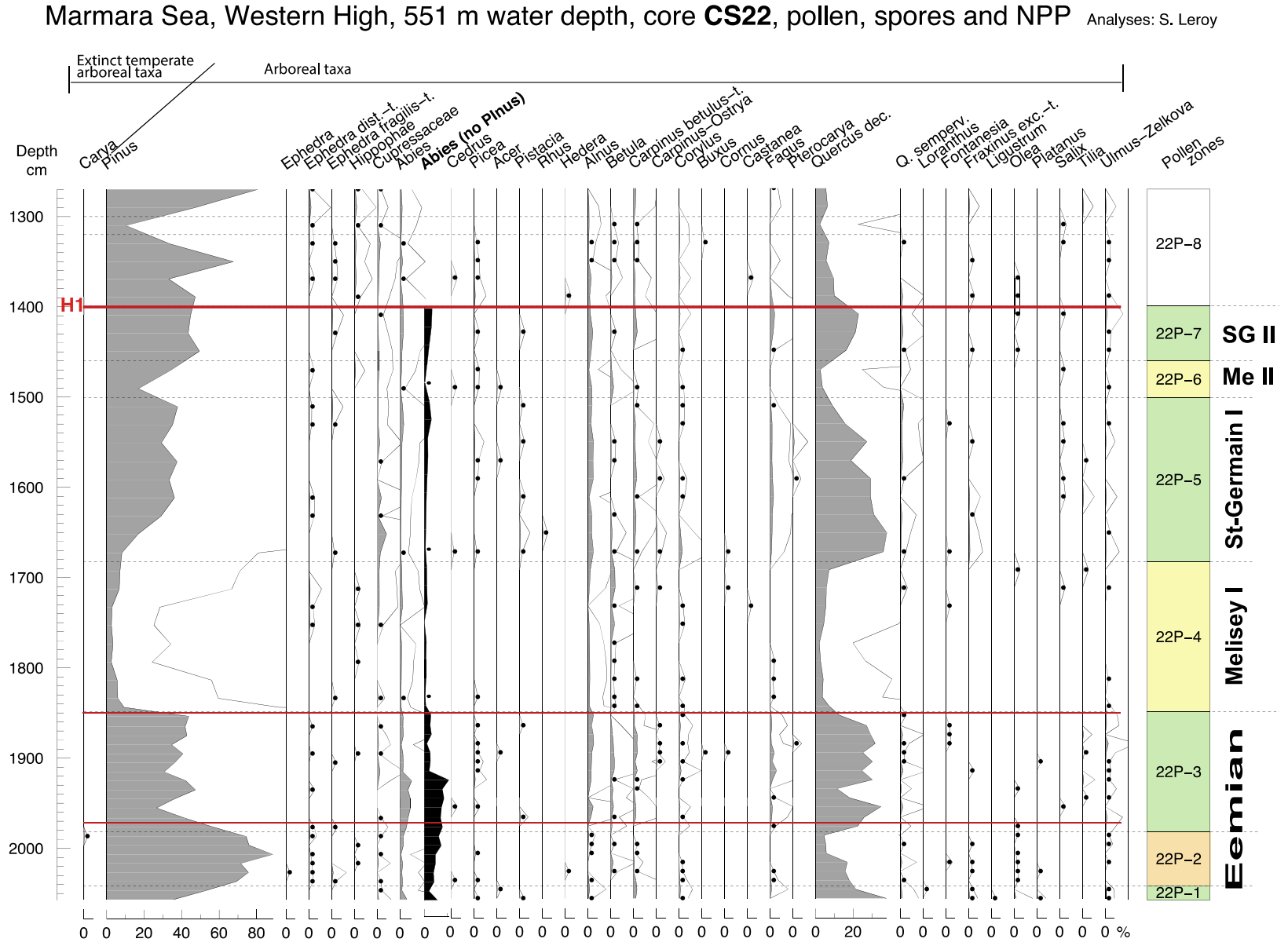
Marmara Sea, Western High, 551 m water depth, core CS22, pollen, spores and NPP
Analyses: S. Leroy
Extinct temperate arboreal taxa
Arboreal taxa
Depth cm
Carya
Pinus
Ephedra
Ephedra dist.–t.
Ephedra fragilis–t.
Hippophaë
Cupressaceae
Abies
Abies (no Pinus)
Cedrus
Picea
Acer
Pistacia
Rhus
Hedera
Alnus
Betula
Carpinus betulus–t.
Carpinus–Ostrya
Corylus
Buxus
Cornus
Castanea
Fagus
Pterocarya
Quercus dec.
Q. semperv.
Lonicera
Fontanesia
Fraxinus exc.–t.
Ligustrum
Olea
Platanus
Salix
Tilia
Ulmus–Zelkova
Pollen zones
1300
1400
1500
1600
1700
1800
1900
2000
H1
22P–8
22P–7
22P–6
22P–5
22P–4
22P–3
22P–2
22P–1
SG II
Me II
St-Germain I
Melisey I
Eemian
0 0 20 40 60 80 0 0 0 0 0 0 0 0 0 0 0 0 0 0 0 0 0 0 0 0 0 0 0 20 0 0 0 0 0 0 0 0 0 0 %

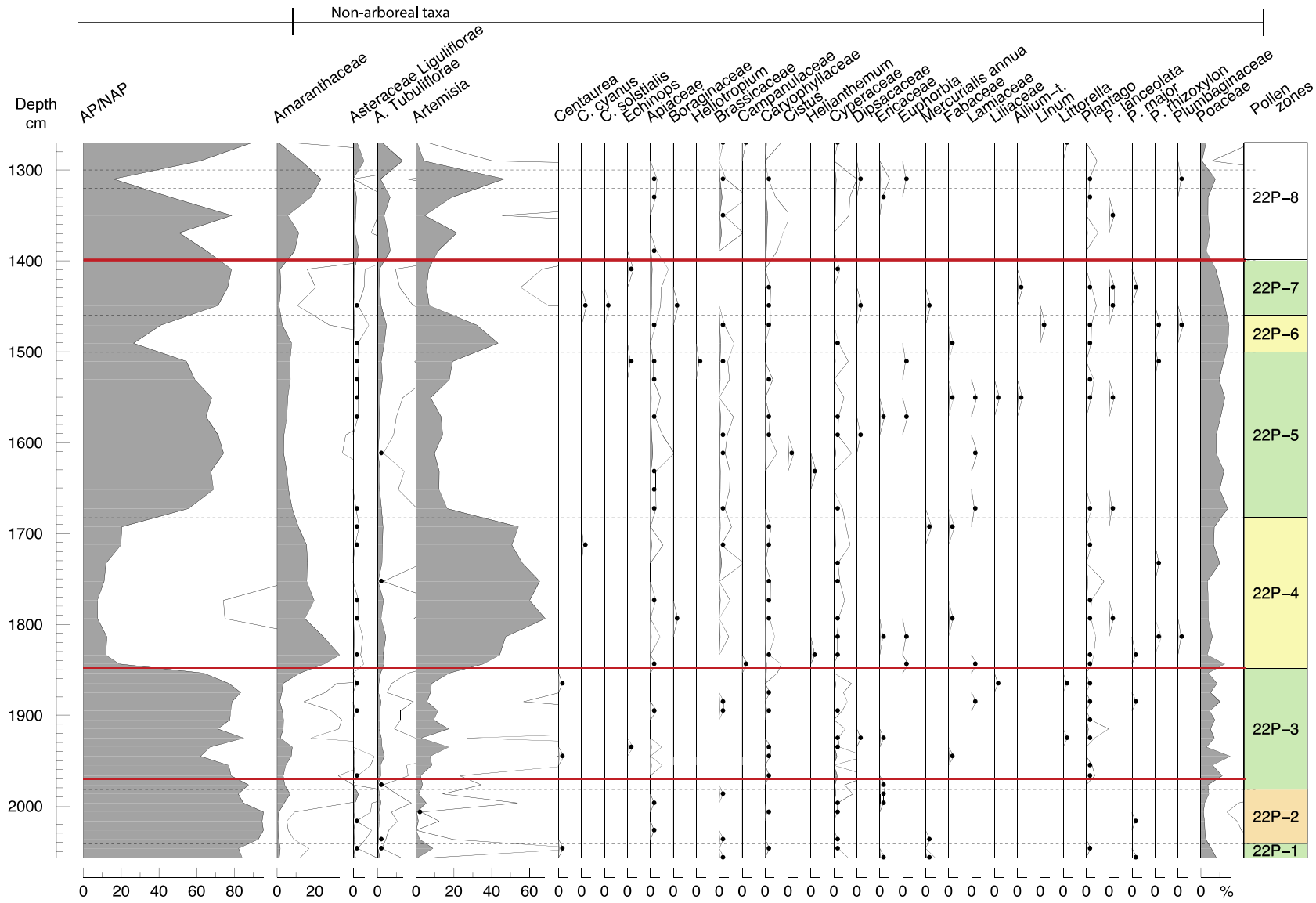
Marmara Sea, Western High, 551 m water depth, core **CS22**, pollen, spores and NPP Analyses: S. Leroy
Non-arboreal taxa
Depth cm
AP/NAP
Amaranthaceae
Asteraceae Liguliflorae
A. Tubuliflorae
Artemisia
Centaurea
C. cyanus
C. solstialis
Echinops
Apiaceae
Boraginaceae
Heliotropium
Brassicaceae
Campanulaceae
Caryophyllaceae
Cistus
Helianthemum
Cyperaceae
Dipsacaceae
Ericaceae
Euphorbia
Mercurialis annua
Fabaceae
Lamiaceae
Liliaceae
Allium–t.
Linum
Littorella
Plantago
P. lanceolata
P. major
P. rhizoxylon
Plumbaginaceae
Poaceae
Pollen zones
1300
1400
1500
1600
1700
1800
1900
2000
22P–8
22P–7
22P–6
22P–5
22P–4
22P–3
22P–2
22P–1
0 20 40 60 80
0 20
0 0
0 20 40 60
0 0 0 0 0 0 0 0 0 0 0 0 0 0 0 0 0 0 0 0 0 0 0 0 0 0 0 0 0 %

Marmara Sea, Western High, 551 m water depth, core **CS22**, pollen, spores and NPP

Analyses: S. Leroy

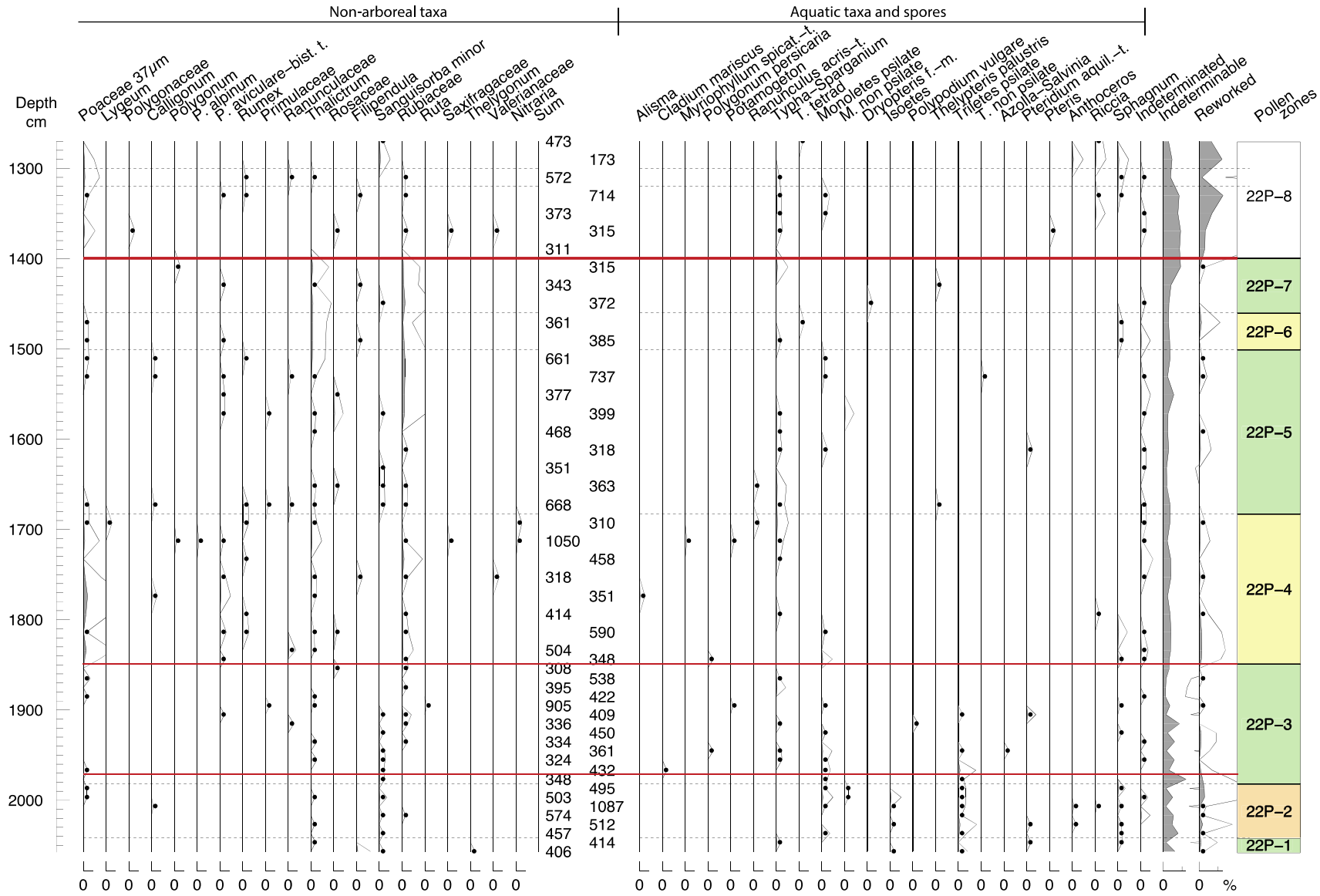

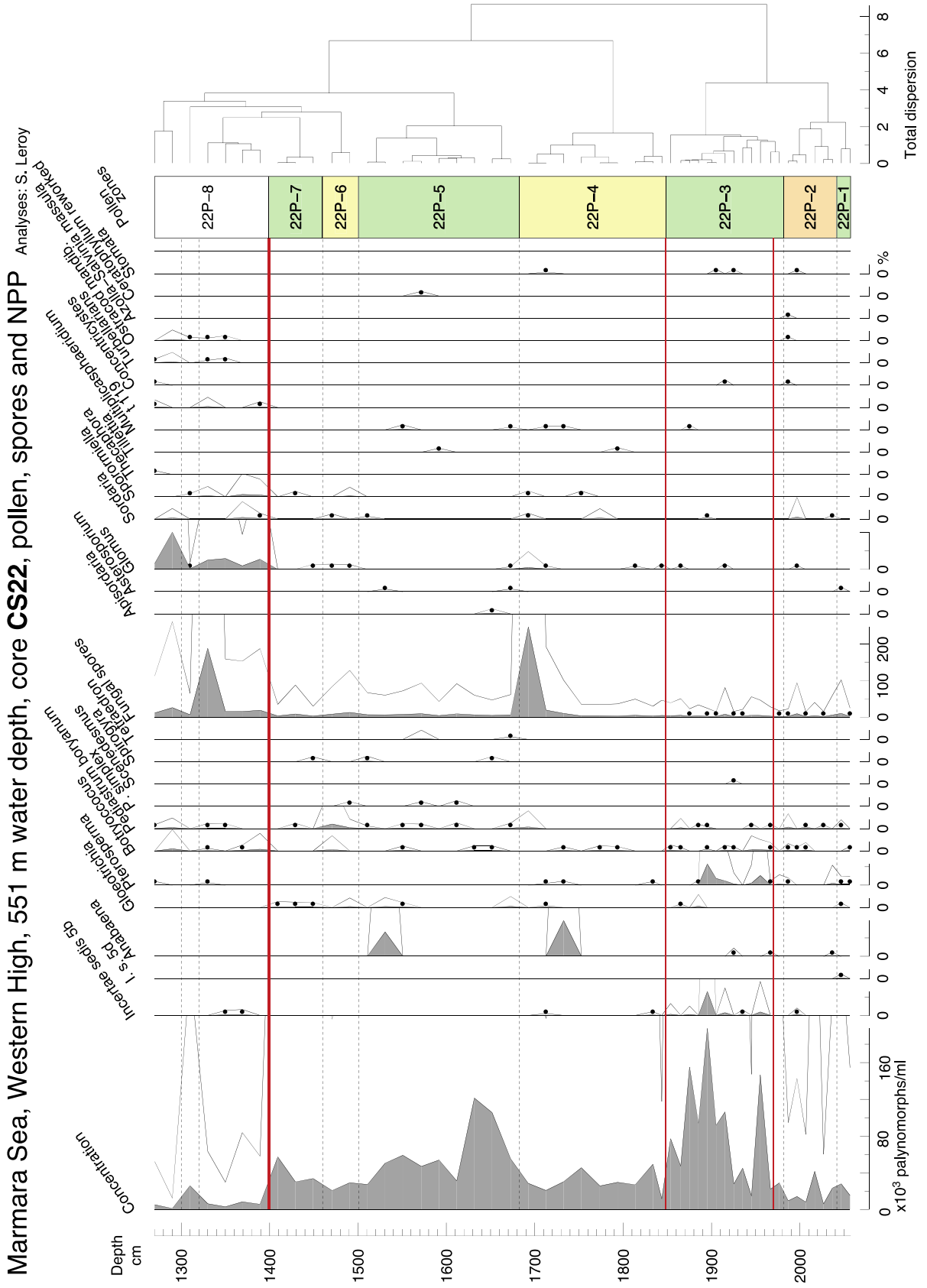

Figure 4: Percentage pollen diagram of core CS22, Western High, 551 m water depth. *Abies* curve is also presented on a sum without *Pinus* (black fill and bold

letters). For the full diagram prepared on a sum without *Pinus* see SI2. Me I = Melisey I Stadial, SG I = Saint-Germain I Interstadial, Me II = Melisey II Stadial, SG II = Saint-Germain II Interstadial.

5.1 Core CS22

Pollen zone 22P-1, 2057-2042 cm depth

Amongst the tree pollen (AP), *Pinus* and deciduous *Quercus* dominate, showing declining values (Fig. 4). *Carpinus betulus, Fagus* and *Olea* are present. In the non-arboreal pollen (NAP), Poaceae, *Artemisia*, Amaranthaceae and some Asteraceae have continuous curves. *Isoetes* are regularly present, a feature unique to this zone and the following. Psilate trilete spores and *Sphagnum* are frequent. Concentration is relatively good, hovering around 20,000 pollen and spores per ml.

Pollen zone 22P-2, 2042-1982 cm depth

This zone is best characterised by a large amount of *Pinus* (up to 89%). Deciduous *Quercus* carry on declining. Less AP are present. For the rest, it is similar to zone 22P-1.

Pollen zone 22P-3, 1982-1849 cm depth

Pinus percentages drop to 40%, while deciduous *Quercus* increase to 30%, with a dip at 1945-1935 cm. Other AP, such as *Abies, Alnus, Betula, Carpinus* and *Fagus* form now continuous curves. The total NAP percentage has only weakly decreased. *Artemisia* values have even increased. Concentrations are maximal, increasing in values above 1920 cm and reaching nearly 200,000 pollen and spores per ml at 1895 cm depth. Incertae Sedis 5b and *Pterosperma* (known also by its fossil name *Cymatiosphaera*) are frequent.

Pollen zone 22P-4, 1849-1683 cm depth

A radical change occurs with pollen zone 4, values of *Artemisia* and Amaranthaceae are very high, up to 68 and 33 % respectively. AP% drop to a minimum. Concentrations have fallen back to around 30,000 pollen and spores per ml. A single peak of *Anabaena* (19 %) at 1732 cm and one of fungal spores (245% of terrestrial pollen) at 1693 cm occur.

Pollen zone 22P-5, 1683-1501 cm depth

Deciduous *Quercus* increase rapidly to a maximum of 38%, whereas *Pinus* increases slowly. Other AP are Cupressaceae, *Pistacia, Alnus, Carpinus*, *Fagus* and some *Pterocarya*. NAP% are low again, but a constant background of *Artemisia* and Amaranthaceae is maintained. A single peak of *Anabaena* (13 %) occurs at 1531 cm. Contrary to zone 3, no Incertae Sedis 5b and no *Pterosperma* are observed. *Pediastrum* simplex has a few occurrences. Concentrations are at first high until 1622 cm, then fall to average values.

Pollen zone 22P-6, 1501-1460 cm depth

This short zone of two samples only is characterised by a fall of the AP owing to a clear increase of *Artemisia* up to 43 %. Poaceae are maximal with 15%.

Pollen zone 22P-7, 1460-1399 cm depth

This is another short zone (three samples), well characterised nevertheless by a re-increase of the AP, especially deciduous *Quercus, Fagus* and *Carpinus*. In the NAP, Poaceae decline slowly across this zone.

Pollen zone 22P-8, 1399-1270 cm depth

Percentages of *Pinus, Artemisia* and Amaranthaceae are sharply fluctuating, while *Quercus* remains around 7% only. *Hippophae* is continuously present. *Ephedra distachya*-t. is frequent. *Anthoceros, Riccia* and *Sphagnum* are common. Concentrations are significantly lower (often lower than 8000 pollen and spores/ml) than the rest of the diagram. Fungal spores are regularly high, including a peak at 187%. *Glomus* are abundant and reach up to 20%. Indeterminable and reworked grains are abundant (up to 9 and 13 % respectively). One observation of *Concentricystes* was made in the topmost sample.

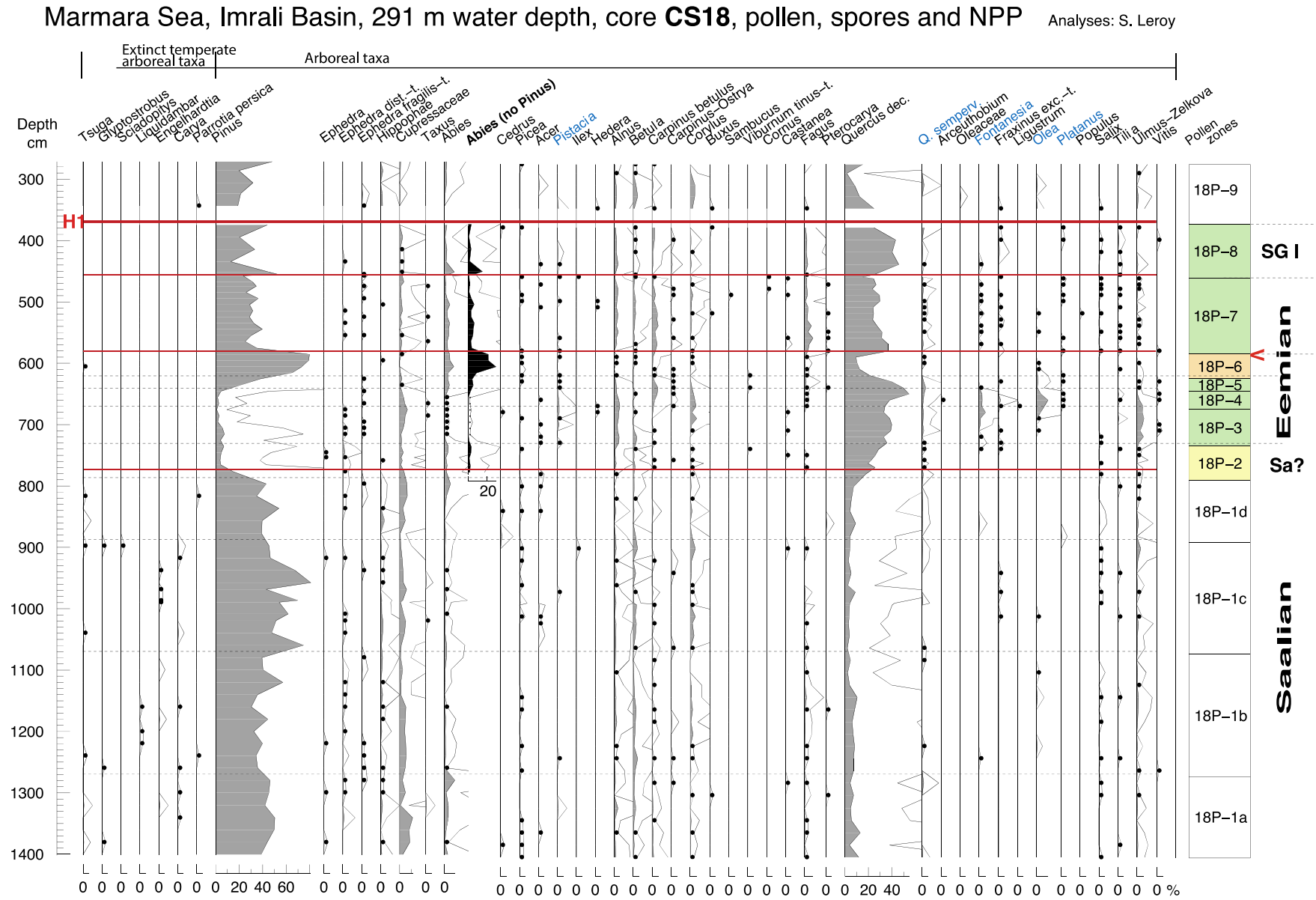
Marmara Sea, Imrali Basin, 291 m water depth, core CS18, pollen, spores and NPP
Analyses: S. Leroy
Extinct temperate arboreal taxa
Arboreal taxa
Depth cm
Tsuga
Glyptostrobus
Sciadopitys
Liquidambar
Engelhardtia
Carya
Parrotia persica
Pinus
Ephedra
Ephedra dist.–t.
Ephedra fragilis–t.
Hippophaë
Cupressaceae
Taxus
Abies
Abies (no Pinus)
Cedrus
Picea
Acer
Pistacia
Ilex
Hedera
Alnus
Betula
Carpinus betulus
Carpinus–Ostrya
Corylus
Buxus
Sambucus
Viburnum tinus–t.
Cornus
Castanea
Fagus
Pterocarya
Quercus dec.
Q. sempery.
Arceuthobium
Oleaceae
Fontanesia
Fraxinus exc.–t.
Ligustrum
Olea
Platanus
Populus
Salix
Tilia
Ulmus–Zelkova
Vitis
Pollen zones
H1
300
400
500
600
700
800
900
1000
1100
1200
1300
1400
20
18P–9
18P–8
18P–7
18P–6
18P–5
18P–4
18P–3
18P–2
18P–1d
18P–1c
18P–1b
18P–1a
SG I
Eemian
Sa?
Saalian
0 0 0 0 0 0 0 0 20 40 60
0 0 0 0 0 0 0
0 0 0 0 0 0 0 0 0 0 0 0 0 0 0 0 0 0 0 20 40
0 0 0 0 0 0 0 0 0 0 0 0 0 0 0 %

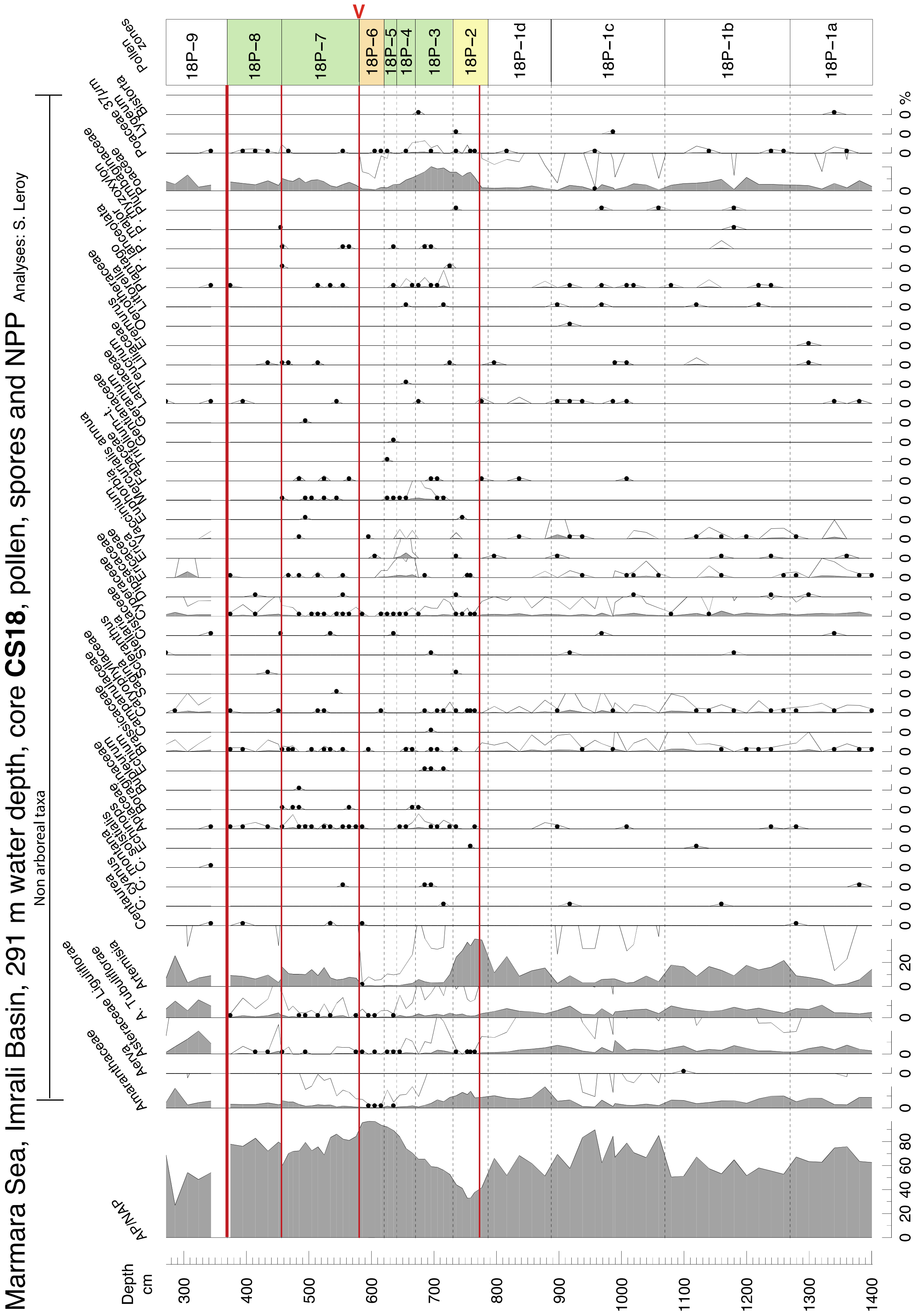
Marmara Sea, Imrali Basin, 291 m water depth, core CS18, pollen, spores and NPP
Analyses: S. Leroy
Non arboreal taxa
Depth cm
300
400
500
600
700
800
900
1000
1100
1200
1300
1400
AP/NAP
Amaranthaceae
Artemisia
Pollen zones
18P–9
18P–8
18P–7
18P–6
18P–5
18P–4
18P–3
18P–2
18P–1d
18P–1c
18P–1b
18P–1a

Marmara Sea,Imrali Basin, 291 m water depth, core **CS18**, pollen, spores and NPP

Analyses: S. Leroy

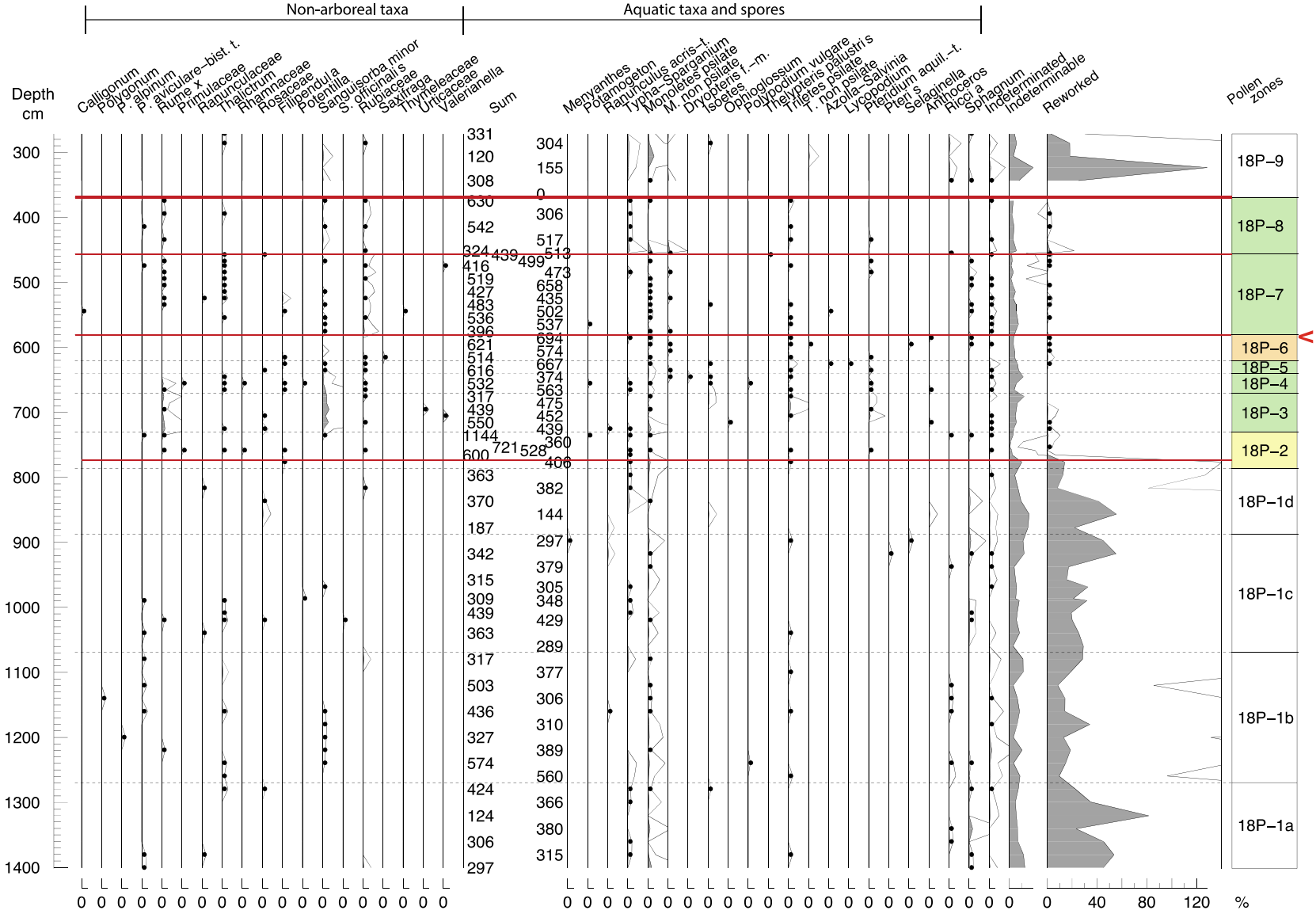

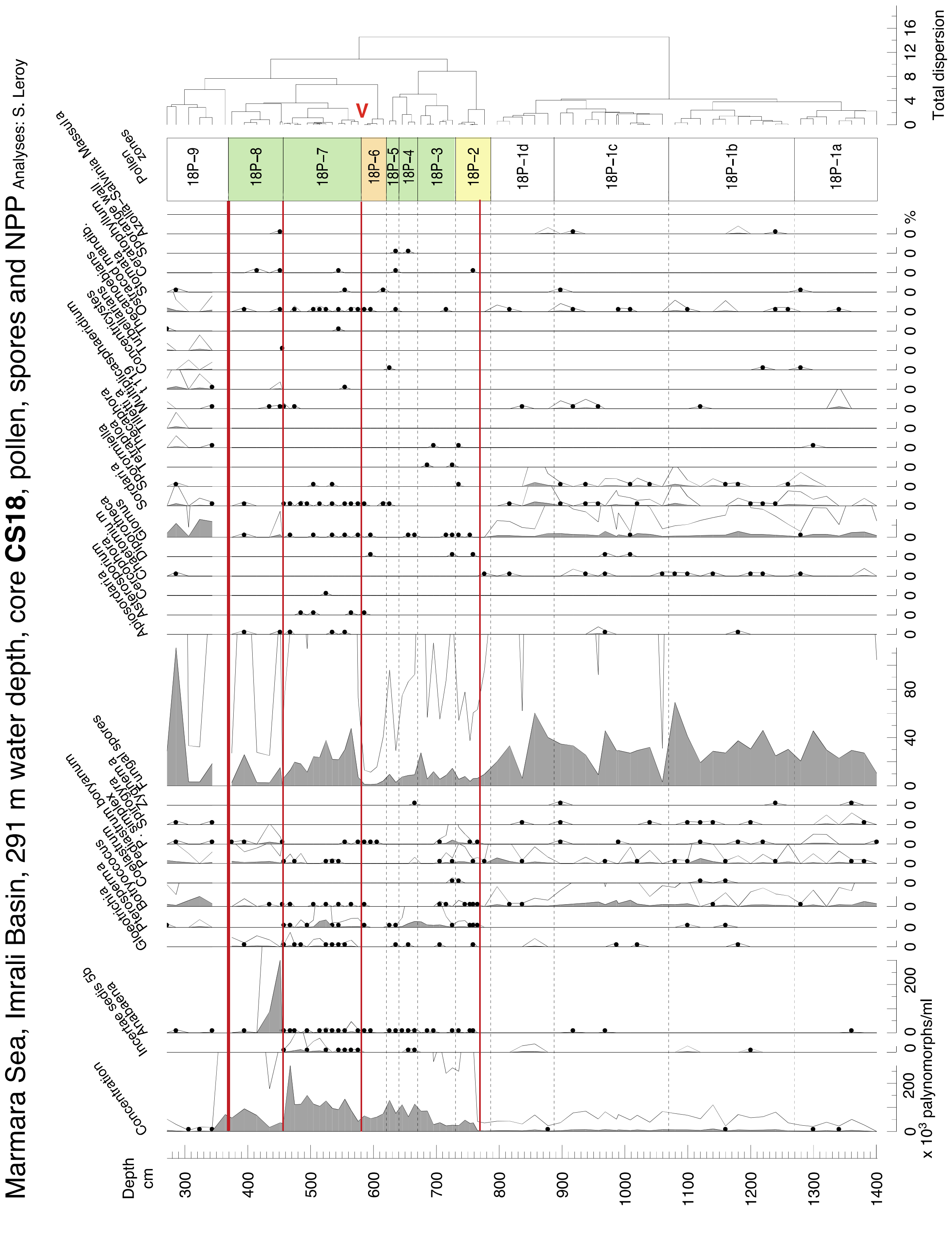

Figure 5: Percentage pollen diagram of core CS18, Imralı basin, 291 m water depth. *Abies* curve is also presented on a sum without *Pinus* (black fill and bold letters). For

the full diagram prepared on a sum without *Pinus* see SI2. SG I = Saint-Germain I Interstadial.

5.2 Core CS18

Pollen zone 18P-1, 1401-787 cm depth

The pollen and spore concentration of this long zone is low, mostly between 2000 and 8000 pollen and spores per ml (Fig. 5). It is dominated by *Pinus* (35-81%), reworked palynomorphs (around 30% with a peak at 81%) and fungal spores (around 30%, up to 70%). In the AP, Cupressaceae and *Hippophae* are continuously present. Deciduous *Quercus* values hover around 5%. In the NAP, *Artemisia*, Asteraceae and Amaranthaceae are well represented. Poaceae values are low, around 5 %. *Botryococcus* and *Pediastrum boryanum* are frequent.
Occasionally tree taxa that have disappeared in Europe and in the Mediterranean region during the Quaternary, such as *Tsuga, Glyptostrobus, Sciadopytis, Engelhardtia, Carya* and *Parrotia persica* or tree taxa that can be found in warmer regions of Turkey such as *Liquidambar,* are present. Zone 1a has more *Abies* and Cupressaceae *(Juniperus-t.)*, zone 1b more *Artemisia* and Poaceae, zone 1c more *Pinus* and *Corylus* and zone 1d more evergreen *Quercus,* Amaranthaceae and *Artemisia*.

Pollen zone 18P-2, 787-731 cm depth

This zone is well characterised by a clear drop of *Pinus* to minimal values and a progressive only increase of deciduous *Quercus*. In the NAP, Amaranthaceae and especially *Artemisia* display high values, respectively of up to 14% and 40%. Poaceae increase across this zone. In comparison to the previous zone, reworked

elements are low and concentrations change from <5000 to > 30,000 pollen and spores per ml in the middle of this zone at 770 cm. Fungal spores are low, below 10%.

Pollen zone 18P-3, 731-671 cm depth

This zone is clearly identified by the development of a range of AP taxa: *Alnus, Quercus* and *Ulmus-Zelkova*. *Betula* makes a bell-shaped curve at the beginning of this zone, while Cupressaceae, *Pistacia, Corylus* and *Fontanesia* increase towards the end of the zone. Evergreen *Quercus* is continuously present in this zone and the two following ones. *Pinus* and *Abies* have minimal values, and *Fagus* is totally absent. The NAP% are rather low, although Poaceae reach a maximum with 20%. *Plantago, Rumex* and *Sanguisorba minor* are continuously present and *Mercurialis annua* increase in the second half of this zone. Concentrations and fungal spore percentages remain as previously. In the NPP, one may note a continuously increasing curve of *Pterosperma*.

Pollen zone 18P-4, 671-641 cm depth

Although short (three samples), this zone is clearly defined. *Pistacia, Alnus, Corylus, Fontanesia* and *Ulmus-Zelkova* are abundant. Deciduous *Quercus* reach a maximum in the top sample: 55%. *Olea* attains a maximum of 10%. *Platanus* has regular single occurrences. NAP%, and especially Poaceae, carry on declining. Several Ericaceae types are present. Concentrations are very high and reach several times >110,000 pollen and spores per ml. No reworking is noted at all. The values of *Pterosperma* are at first maximal (5%) and then drop.

Pollen zone 18P-5, 641-621 cm depth

This very short zone (two samples) is justified by the sharp increase of *Pinus*, falling values of deciduous *Quercus* and the redevelopment of *Abies*. Many AP types decline. NAP% remain low. Poaceae carry on declining.

Pollen zone 18P-6, 621-581 cm depth

Pinus values are very high and reach a maximum of 80%. *Abies* values are high: up to 8%. The other AP are low, including *Quercus*. All NAP values are low too, including Poaceae that reach their minimal values.

Pollen zone 18P-7,581-456 cm depth

After a sharp change, *Pinus* values are now at 30% only. *Abies* is still well represented. Diverse AP taxa re-appear: deciduous *Quercus, Alnus, Betula* and *Corylus*. To be noted, the abundance of *Carpinus* and *Fagus*. In the NAP, *Artemisia* and Poaceae reincrease up to 15% and 10% respectively. Concentrations are exceptionally high, often around 100,000 palynomorphs per ml, with a peak at 273,000 palynomorphs per ml. Incertae Sedis 5b is quasi continuous. In the zone middle, a clear bell-shape curve of *Pterosperma* appears.

Pollen zone 18P-8, 456-369 cm depth

After another sharp change, the first sample bears special characteristics: with peaks of *Abies, Typha-Sparganium*, psilate monolete spores, non-psilate monolete spores, reworked elements, *Anabaena* (301% of terrestrial pollen) and *Glomus*. The rest of this zone is dominated by deciduous *Quercus* and *Pinus*. *Pterocarya* is remarkably absent. In the NAP, *Artemisia*, Poaceae and Cyperaceae form the bulk of the percentages. Concentrations are back to average. *Gloeotrichia* and *P. simplex* are common, while Incertae Sedis 5b and *Pterosperma* are absent.

Pollen zone 18P-9, 369-272 cm depth

The first sample of this zone is barren, as taken in a horizon containing possible shell clusters. The rest of this zone resembles somewhat zone 1, without however the taxa that went extinct in Quaternary. The AP values are relatively low, dominated by *Pinus* and deciduous *Quercus*. In the NAP, Asteraceae are abundant. Reworked elements are abundant to extremely abundant (up to 128%) and fungal spores up to 114%. *Glomus* is very important in most samples. *Concentricystes* is frequent.

5.3 Climatic reconstruction from cores CS22 and CS18

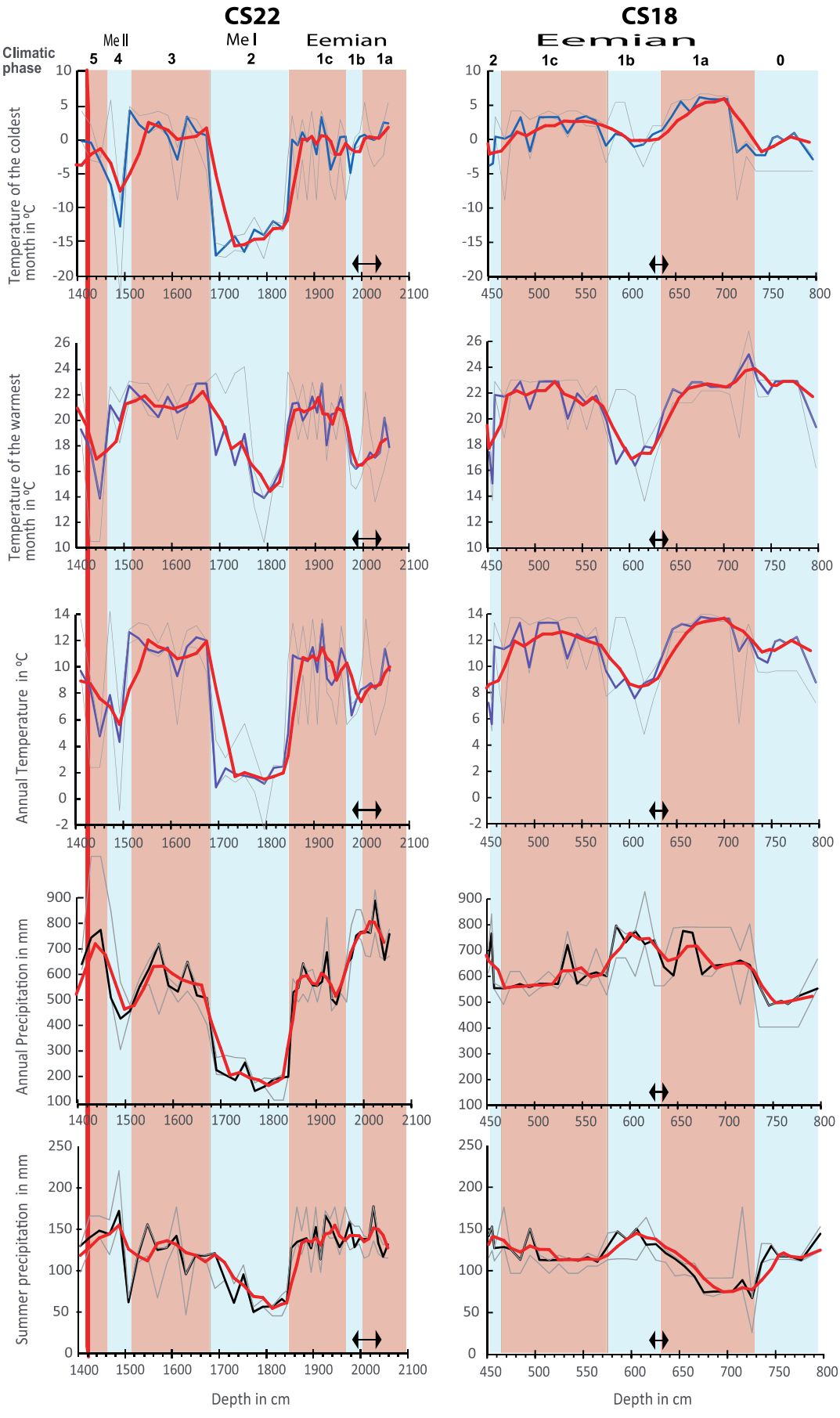
CS22
CS18
Climatic phase
Me II
Me I
Eemian
5
4
3
2
1c
1b
1a
2
1c
1b
1a
0
Temperature of the coldest month in °C
Temperature of the warmest month in °C
Annual Temperature in °C
Annual Precipitation in mm
Summer precipitation in mm
Depth in cm
Depth in cm
Pinus zone
Me I, Me II: Melisey Interstadials I and II

Figure 6: Climate reconstruction inferred from cores CS22 and CS18. The Modern Analog Technique (MAT) has been used to reconstruct the temperature of the coldest month, the temperature of the warmest month, annual temperature and annual precipitation. For each climate parameter, mean values and error ranges are plotted in blue, and the moving average is plotted in red. Red zones corresponds to warm phases and blue zones corresponds to cold phases. The dotted red line shows the red-H1 hiatus.

Based on the MAT approach, the climatic reconstructions for both cores CS22 and CS18 show comparable values along the last interglacial period (Fig. 6).

Core CS22: Five climatic phases have been defined and are described below.
Phase 1 (2057-1849 cm depth) is marked by warm (annual temperature above 10°C) and humid climate conditions (600 to 800 mm); summers were also humid (120 to 150 mm). The beginning of this zone (2057-2000 cm) is the wettest of the sequence. An abrupt event named 1b characterised by cold and dry conditions is evidenced between 2000 and 1960 cm. The *Pinus* zone (22P-2) displays a cooling trend and a slight decrease from the preceding humid conditions. Then the temperature and the precipitations increase.
Phase 2 (1849-1683 cm depth) shows a long climate period marked by cold and very dry conditions. The drop in temperatures is around 10°C and the precipitations are low, around 200 mm only.

Phase 3 (1683-1501 cm depth) is comparable to phase 1, with warm and humid conditions. Temperatures are high (around 12°C), but precipitations are lower than during phase 1 (around 600 mm).
Phase 4 (1501-1460 cm depth) is a short period mainly characterized by a drop in temperatures and precipitations. This phase is less cold and dry than phase 2.
Phase 5 (1460-1400 cm depth) is marked by a temperature increase and high amplitude climate oscillations with values below 10 °C, lower than those recorded during phases 1 and 3.

Core CS18: Three climatic phases have been defined and are described below. Phase 0 (787-730 cm) is characterised by warming temperatures (except in winter) and low precipitations. Phase 1 (730-456 cm depth) is marked by clearly warm and humid conditions, comparable to those evidenced in core CS22 phase 1, with temperatures close to 12°C, interrupted by a cold/wet event. The temperatures increase and they reach an optimum around 680 cm (phase 1a). Precipitation also increases during phase 1a and reach 800 mm but summer precipitations were low (80 mm) at the onset of phase 1a. A first abrupt event named 1b marked by cooler and dryer conditions, but precipitations remain high (also during summers). This cold event suggests a pattern comparable (trend and values) to the event depicted in core CS22 (phase 1b). The *Pinus* zone (18P-6) is at the beginning of this phase. It is characterised by warm and humid conditions. In phase 1c, the temperatures are high (around 12°C) but slightly lower than values reconstructed in phase 1a, and precipitation decreases but remains high. Phase 2 (≤ 456 cm depth) is mainly characterized by a drop in temperatures.

6 Interpretation and discussion

6.1 Taphonomic effects in the two diagrams

Strong negative and positive taphonomic effects are observed in both cores. The negative ones may be classified in two different types, i.e. at the level of the pollen zones and by sharp assemblage changes.

Three zones, 18P-1, 18P-9 and 22P-8, are especially concerned. Zone 18P-1 has low concentration, the occurrence of oxidation-resistant taxa such as Asteraceae and many reworked elements. In zone 18P-9, an even stronger taphonomic imprint is observed as testified by the additional occurrences of *Glomus* (soil erosion) and *Concentricystes* (erosion along river shores). In zone 22P-8, the pollen spectra are clearly affected by reworking: low concentration, abundance of Asteraceae and reworked elements. *Glomus* here too implies strong soil erosion. The water level in these three zones - with an oxidation-prone sedimentation environment - was probably shallow. The relatively frequent pollen grains of regionally extinct trees (*Tsuga, Glyptostrobus, Sciadopytis, Liquidambar, Engelhardtia, Carya* and *Parrotia persica)* in zone 18P-1 is most likely due to erosion and river transport (Fig. 5). This core is in the area under influence of the delta of the Kocasu, when water levels are low. The much larger number of reworked elements in zone 18P-9 than in the equivalent zone 22P-8 (both above the red-H1seismic reflector horizon) is explained in the same way: i.e. by river influence.

The two pollen diagrams show some very sharp changes between some zones as illustrated by the jump in the dispersion values obtained by CONISS. They are often accompanied by a sand or a silt layer (e.g. red lines in figures 2, 3, 4 and 5). In addition, the first sample of zone 18P-8, at 455 cm depth, is heavily marked by

erosion and transport: *Pinus, Abies*, Asteraceae, *Typha-Sparganium*, psilate and non-psilate monolete spores, indeterminable and reworked palynomorphs, *Anabaena, P. simplex, Glomus* and some other taxa form an anomalous peak. This mixed assemblage of heavy, oxidation-resistant and/or freshwater taxa clearly reflects a mass-wasting event with a strong contribution from the shores and the initiation of new aquatic conditions in the SoM. Still in core CS18, sample at 369 cm, thus just above the red-H1 reflector, is barren.

On the contrary, a positive taphonomic influence occurs owing to the deposition of finely dark laminated clays in both cores, forming under reducing environments. In zones 22-P3 and 18P-7, pollen concentrations are indeed very high (respectively >190,000 and >270,000 pollen per ml). This exceptionally good pollen preservation in sapropel has been noted elsewhere too (Cheddadi and Rossignol, 1995; Çaner and Algan, 2002; Kotthoff et al., 2008).

6.2 Vegetation reconstruction from the two Marmara sequences

Vegetation reconstruction from core CS22 shows first in zone 22P-1 a forest steppe (pine and oaks), that becomes a purer pine forest in zone 2. After a sudden change, a diverse deciduous forest with an Euxinian character is established in zones 22P-3, 5 and 7, i.e. dominant oaks with *Carpinus betulus* and *Fagus*. Zone 22P-3 has a maximum of *Abies*, a conifer tree from precipitation-facing mountain slopes, here north-facing slopes of surrounding mountains. In zone 22P-4, an *Artemisia* steppe develops alongside some semi-desertic areas (Amaranthaceae), whereas in zone 22P-6 some pine stands persist in an *Artemisia* steppe and some grasslands. After another strong change, zone 22P-8 displays again a very open landscape.

Concerning core CS18, in the long zone 18P-1, the pine woodland was strongly developed with some *Artemisia* steppe in drier places. In zone 18P-2, the assemblages reflect a milder environment. An *Artemisia* steppe has developed with some oaks, although in places the environment is a grassland. The maximum of Amaranthaceae could be due either to saline soils or to coastal marshes. Zones 18P-3 to 5 allow reconstructing an interglacial with a clear Mediterranean character *Fontanesia, Olea, Platanus, Pistacia* and evergreen-t. *Quercus*) and vegetation succession. Zone 18P-3 reflects a humid forest establishment with riparian forest with alder and elms alongside an oak forest. Towards the end of this zone, a Mediterranean climate sets in with the expansion of olive trees and evergreen oaks. In zone 18P-4, the Mediterranean character of the forest is strongest. Zone 18P-5 indicates that pines are progressively re-expanding and replacing the oak forest. Zone 18P-6 has a clear maximum of pine forest expansion to the detriment of all other trees, except the montane conifer *Abies* and deciduous *Quercus*, suggesting that the fir belt extended downwards on the mountain slopes. In zones 18P-7 and 8, the oak forest is back, but the forest cover is not very dense, allowing for patches of pine and *Artemisia*. *Carpinus betulus* and *Fagus* have their maximal development in zone 18P-7. *Pterocarya* is frequent, giving an Euxinian touch to the forest in zone 18P-7; but it is clearly absent from the following zones. Zone 18P-9 (after a barren sample at 369 cm) is very similar to zone 18P-1. Despite taphonomic issues, one may reconstruct an open landscape from these spectra.

6.3 Core correlation and proposed chronology

6.3.1 Correlations based on geo-physico-chemical data

For the purpose of a detailed correlation between cores below the red-H1 reflector, the density, TOC and Ca values of the three cores are compared (Fig. 3). In general, density shows sandy layers as peaks and hiati as discontinuities. Ca values reflect the Ca content of the sediment and is therefore a reflection of endogenic carbonate production related to changes in palaeoceanographic condition in the SoM. The exceptions are some high values associated with lacustrine shelly layer that are preserved such as at 1960 cm in core CS27. Quite significantly, the high Ca values at 1575-1510 and 1450-1400 cm in core CS22 are most likely absent in core CS27 and all the more so from core CS18.

Overall, the silty-sandy layers are thinner and finer in core CS22, and their interpretation as hiati is less compelling. From the west to the east of the SoM, progressively less sediment is preserved and hiati become more important. Some hiati are common to the three cores (thus across c.100 km and two basins) not only the red-H1 reflector, but also 1840 cm in core CS22 (small fault), with 1960 cm in core CS27 (shell-rich sand) and 445 cm in core CS18 (sand) (Fig. 3). Finally another cross-correlation is at around 1980-1940 cm in core CS22 (many microfaults below 1970 cm) and 570 cm in core CS18.

The inter-core correlation suggests most events are not local but have affected at least one basin or the whole SoM. The cause of these hiatus cannot be formally identified; but they are likely to be linked to earthquakes on the North Anatolian Fault and/or sea level changes. In addition, core CS18, located on a slope, may furthermore be affected by mass-wasting events.

Most of the correlations plotted on figure 3 correspond to the above-described pollen zone limits. Moreover geochemical correlations (peaks of TOC) suggest two additional limits in core CS22. These are close to 1925-1915 cm and 1631-1611 cm where a sudden increase in pollen concentration occurs (Fig. 4 and 5).

6.3.2 Eemian Interglacial (c. MIS 5e)

In pollen diagrams, the Eemian Interglacial with its usual warmer-than-present temperatures is commonly rather easily distinguished from successive interstadials. Hence it may consist as a starting point in the absence of dating (such as tephras and radiocarbon dates used further upcore).

The occurrence of Mediterranean pollen taxa (e.g. *Olea* pollen grains), the absence of *Fagus* and the occurrence of Ericaceae (most likely Mediterranean species) in zones 18P-3 to 5 present a strong similarity with the Pangaion or Eemian Interglacial in the pollen diagram of Tenaghi Philippon (Milner et al., 2013, 2016) and to other Mediterranean records showing a characteristic peak of sclerophyllous vegetation at that time such as the Dead Sea, Yammoûneh, Lake Van, Ioannina basin, Lago de Monticchio (Chen and Litt, 2018). These three short pollen zones are therefore attributed without ambiguity to the Eemian Interglacial.

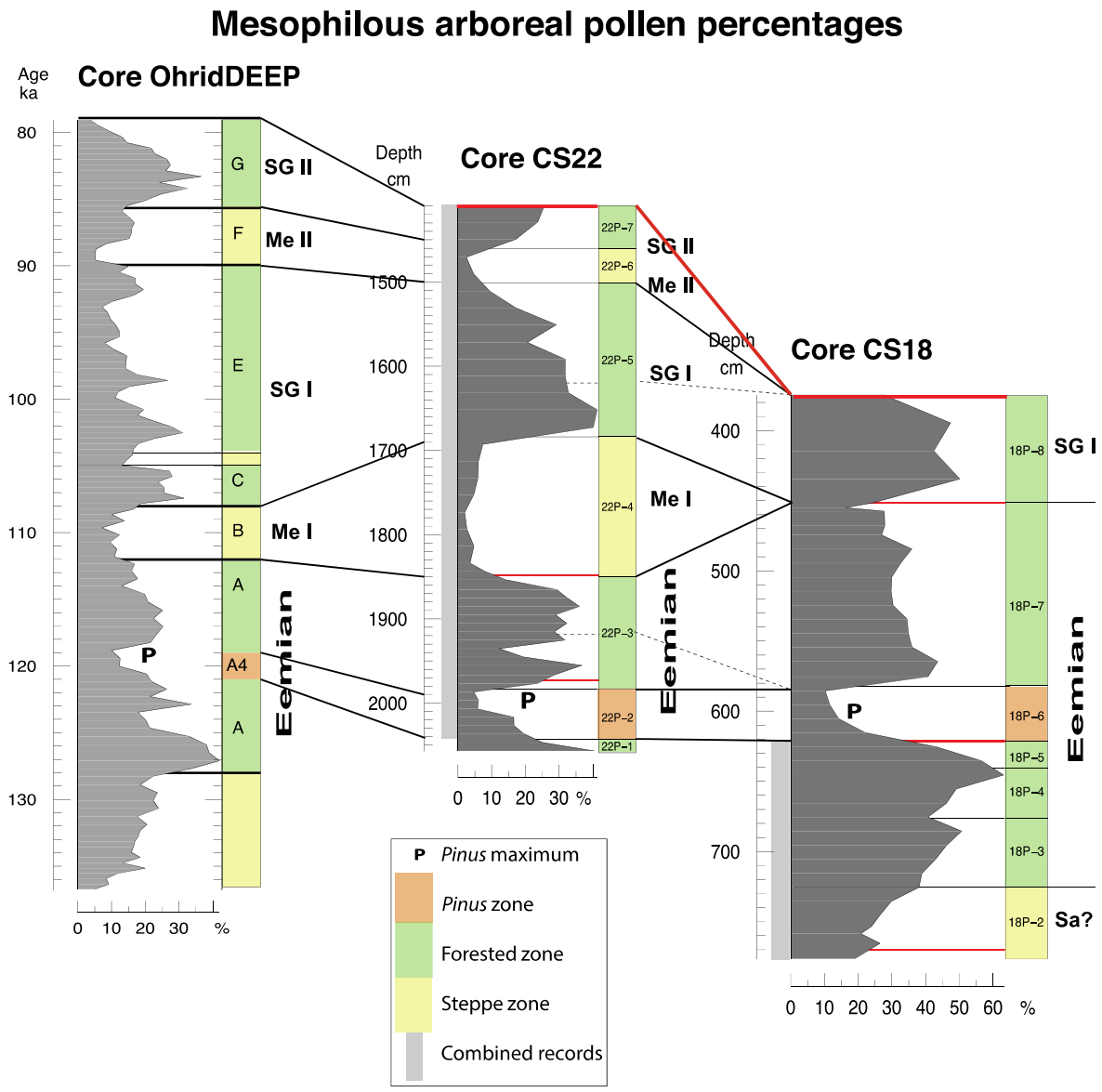

Figure 7: Curves of mesophilous pollen percentages (as defined in Sinopoli et al., 2019) for the OhridDEEP core and the two Marmara cores. P = peaks in *Pinus* percentages. Me I = Melisey I Stadial, SG I = Saint-Germain I Interstadial, Me II = Melisey II Stadial, SG II = Saint-Germain II Interstadial.

The two Marmara pollen diagrams were redrawn with percentages made on a sum without *Pinus* (a strong pollen producer) in order to highlight the other taxa present in these assemblages (*Abies* curves in percentages built on a sum without *Pinus* in Fig. 4 and 5 and whole diagram without *Pinus* in supplementary information

SI2), especially in the *Pinus* zone (22P-2 and 18P-6, respectively 90 and 80%) seen in both cores. This clearly brings out the high values of deciduous *Quercus* and *Abies* in most of zones 22P-2 and the whole of zone 18P-6. In addition, zone 22P-2 appears to end with two samples with slightly higher NAP values reflecting a brief colder phase (phase 1b in figure 6). It is proposed to correlate these two zones to the pine maximum at the end of Pangaion Interglacial in Tenaghi Philippon and to the *Pinus* maximum (zone A4) of the Ohrid sequence (Sinopoli et al., 2019), as indicated on Figure 7 that displays the curves of mesophilous pollen percentages (as defined in Sinopoli et al., 2019) for the OhridDEEP core and the two Marmara cores. The vertical distributions of warm-loving dinocysts and of a seasonal-contrast dinocyst indicators (outlined in Fig. 8) suggest also a mild climate. Therefore, this *Pinus* wood or even forest phase is interpreted here as a continental period within the Eemian Interglacial rather than a cold-dry stadial (Leroy et al., accepted). The two *Pinus* zones (zones 22P-2 and 18P-6) reflect a vegetation probably dominated by *P. nigra* (growing in more humid conditions than *P. brutia*), although species attribution is impossible.

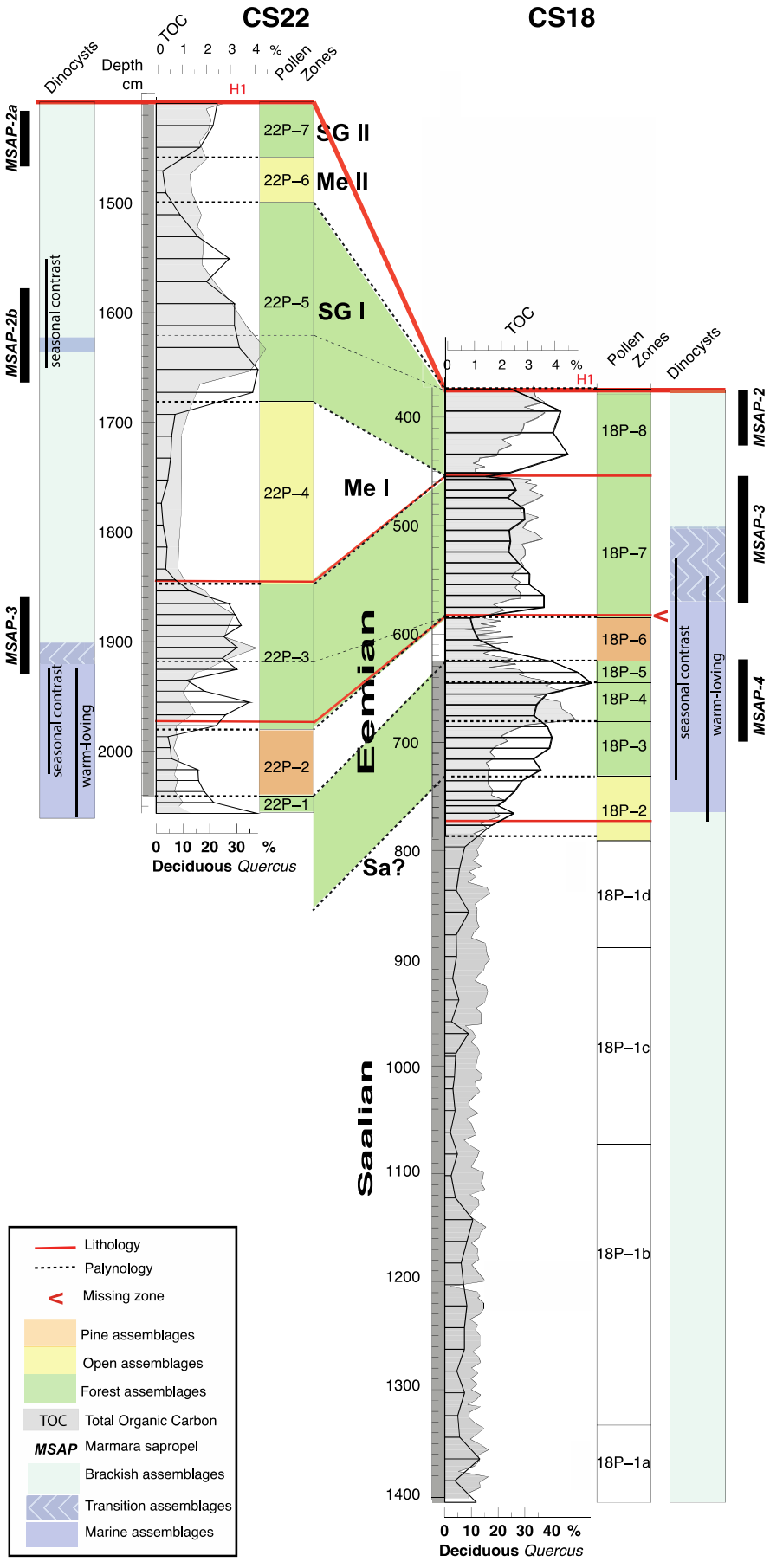
CS22
CS18
Dinocysts
Depth
cm
TOC
0 1 2 3 4 %
Pollen
Zones
H1
MSAP-2a
MSAP-2b
MSAP-3
seasonal contrast
warm-loving
22P–7
22P–6
22P–5
22P–4
22P–3
22P–2
22P–1
SG II
Me II
SG I
Me I
Eemian
Sa?
Saalian
1500
1600
1700
1800
1900
2000
400
500
600
700
800
900
1000
1100
1200
1300
1400
0 10 20 30 %
Deciduous Quercus
18P–8
18P–7
18P–6
18P–5
18P–4
18P–3
18P–2
18P–1d
18P–1c
18P–1b
18P–1a
MSAP-2
MSAP-3
MSAP-4
0 10 20 30 40 %
Deciduous Quercus
Lithology
Palynology
Missing zone
Pine assemblages
Open assemblages
Forest assemblages
TOC Total Organic Carbon
MSAP Marmara sapropel
Brackish assemblages
Transition assemblages
Marine assemblages

Figure 8: Inter-core correlation (CS18 and 22) for MIS 5 based on deciduous *Quercus* percentages. The Total Organic Carbon (TOC) curves appear in grey fill in the background. Me: Melisey Stadial, SG: Saint-Germain Interstadial, Saal: Saalian Glacial. Black lines for pollen correlations. Red lines for hiatus. Me: Melisey Stadial, SG: Saint-Germain Interstadial. Green zone filling for forest cover, Orange zone filling for *Pinus* forest and Yellow zone filling for open vegetation cover. Dinocysts: pale blue boxes for brackish assemblages, dark blue boxes for marine assemblages. Dinocyst taxon list in SI1. Horizontal bold V for pollen and dinocyst zones absent in core CS18. By combining the two light grey vertical boxes, the most complete record is obtained.

Zones 22P-3 and 18P-7 are suggested to be the end of the Eemian as the dinocysts show the transition from marine (>95% and >60% in respective core) to brackish (>95% and >60% respectively) conditions illustrating the drop of water level close to the end of the interglacial. Shackleton et al. (2003) have shown that the sea level of MIS 5e drops before the end of the Eemian per se.

MIS 5e is more completely represented in core CS18, but nevertheless it seems not whole on the base of a maximum of *Abies* in the first half of zone 22P-3 that is not recorded in zone 18P-7. This missing zone is supported by a dinozone with high percentages of cysts of *Pentapharsodinium dalei* and cysts of *Scrippsiella trifida* in core CS22 absent at 580 cm in core CS18 (horizontal red and bold V in Fig. 8) (Leroy et al., accepted).

6.3.3 Saint-Germain Interstadials and Melisey Stadials (MIS 5d to 5a)

Following the recognition of the Eemian Interglacial, the overlying zones 22P-4, 5, 6 and 7 are suggested to be Melisey I Stadial, Saint Germain I Interstadial,

Melisey II Stadial and Saint-Germain II Interstadial. This option is indeed chosen amongst other possibilities (including for example Ognon Interstadials equivalent to Greenland interstadials G19 and G20 in the Greenland Ice Core chronology) as being by far the most parsimonious, considering that the hiati below the red-H1 marker are minor and that the largest loss of sediment must be attributed to the red-H1 seismic horizon, due to its substantial regional importance.

Pollen zone 18P-8 is an interstadial whose age attribution may be constrained with a geochemically-based correlation: at the very top of core CS22, the highest total Ca values of the two cores occur (Fig. 3), while organic carbon content remains in the 2-3 % range (Fig. 2). This geochemically-identified layer, corresponding to pollen zone 22P-7, is thus a carbonate- and organic-rich layer that has no equivalent in core CS18. This, and the correlation proposed between the two cores from the Imralı Basin, i.e. core CS27 and core CS18 based on Ca peaks and organic carbon content (Çağatay et al., 2019), suggests that a possible carbonate-rich layer (top of MSAP-2, Fig. 2) was indeed removed by erosion in core CS18. Thus, zone 18P-8 cannot be Saint-Germain II but must be older, i.e. Saint-Germain I (thus equivalent to zone 22P-5).

Another important point is that the low-arboreal-pollen – high-*Artemisia* interval 22P-4 does not have an equivalent in core CS18 (Fig. 8). This >1.6 m-long interval, corresponding to a very cold and dry period, may have been removed by erosion too. According to correlations above and below, the sand layer at 451 cm in core CS18 matches this interval. Based on other proxies, including the occurrence of *Dreissena* shell fragments and some reworking, Çağatay et al. (2019) suggests the presence of a stadial, even if much reduced. The resolution of the pollen diagram at that depth does not allow to clearly identify a stadial. A corresponding hiatus is

present at the base of the 22P-4 interval in core CS22. The CONISS zonation in core CS22 shows the main change of the diagram at that depth (Fig. 4). It is where silt layers and syn-sedimentary core disturbances are found.

6.3.4 Saalian Glacial (c. MIS 6) and Saalian-Eemian limit

For the sake of completeness, it is important to indicate that, in the absence of a major hiatus, zone 18P-1 is therefore reasonably attributed to the whole or to a large part of the Neakaterini Glacial in Tenaghi Philippon (Wijmstra and Smit, 1976) or Saalian Glacial (roughly equivalent to MIS 6, 191-130 ka ago; Lisiecki and Raymo, 2005).

Zone 18P-2 is a zone illustrating an *Artemisia* steppe (thus possibly part of a glacial period). However, the marine waters from the Mediterranean Sea were already flowing eastwards towards the Black Sea, as established by a dinocyst-based reconstruction of surface waters in the same core with assemblages containing warm-loving dinocysts (Fig. 8 and details in Leroy et al., accepted.). This suggests that this short period with an *Artemisia* steppe, reflecting a dry climate, developed during a period when global sea level was rising due to globally increasing temperatures and surface waters were already significantly warming. Thus, zone 18P-2 possibly already belongs to the interglacial and would illustrate a dry phase at the initiation of the Eemian Interglacial. As a consequence, this is questioning where to put the limit between the Saalian Glacial and the Eemian Interglacial in core CS18. The question remains open.

6.4 Comparison to other pollen sequences

A Mediterranean vegetation is found preferably in MIS 5e, not only in Marmara core CS18, but also in Tenaghi Philippon, Ioannina and Ohrid (Tzedakis et

al., 2001; Milner et al., 2016; Sadori et al., 2016; Sinopoli et al., 2018). Ericaceae display a peak in Tenaghi Philippon stage MIS 5e, as well as here (Milner et al., 2016). In comparison to the Eemian pollen diagram from Bulgaria, the Marmara one is different as the first part of the Eemian (zones 18P-3 to 5) has more Mediterranean taxa. Concerning the second part of the Eemian (zone 18P-7) and the following interstadial (zone 18P-8), more similarities are noted. However, the Marmara sequence displays a strong dominance of oak, leaving less space for other deciduous taxa such as *Carpinus betulus* and *Alnus* (Bozilova and Djankova, 1976). A comparison to the pollen diagram of core 22-GC3/8 in S-E Black Sea evokes similar observations: Mediterranean taxa at the beginning of the interglacial, more dominance of oaks in the Marmara site, and a more even share between deciduous taxa in the S-E Black Sea diagram (Shumilovskikh et al., 2013).

The glacial and stadial vegetations are best revealed in zones 18P-2 (end of Saalian), 22P-4 (Melisey I), 22 P-6 (Melisey II) and, less so, in zone 18P-1 (Saalian) as it is very much affected by differential preservation and reworking. The cold and dry periods of the two Marmara sequences display very open landscapes of an *Artemisia* steppe, where the tree presence is extremely reduced. It mainly falls below 40 % in core CS18 (end of Saalian) and even below 20% in core CS22 (Melisey I). The arboreal spectra are mostly reduced to *Pinus* and deciduous *Quercus* in core CS22, with, in addition, some *Ephedra*, Cupressaceae (*Juniperus-t.*) and *Abies* in core CS18.

During the Saalian Glacial, the vegetation of Tenaghi Philippon (Wijmstra and Smit, 1976) is an *Artemisia* and Amaranthaceae steppe, with some milder periods showing a minor forest-steppe (oak and pine) development in the first part of the glacial only. In the Lake Ohrid sequence, a steppe vegetation prevailed during MIS 6

(Sinopoli et al., 2018). The first part (*Artemisia* steppe rich in Poaceae) has extremely high sedimentation rates due to very strong erosion (Francke et al., 2016). Its second part (*Artemisia* steppe with considerable amounts of *Juniperus*) is very dry (the driest of the last 500 ka) and has low lake levels (Sadori et al., 2016). In Ioannina (Roucoux et al., 2011), a bipartite MIS 6 was also recognised with the first part of the glacial period maintaining moderate presence of temperate trees, and a second part with a clearly smaller tree population and a steppe expansion.

In core CS18, it may be suggested that a first part of the Saalian displays a forest-steppe in a very erosive environment (zone 18P-1). It is followed by a brief drier glacial environment (zone 18P-2) when erosion dramatically drops and an *Artemisia* steppe develops. Despite a strong taphonomical imprint (not only in the SoM), the SoM glacial sequence thus offers some similarities to the bipartite Ohrid, Tenaghi Philippon and Ioannina glacial sequences.

6.5 *Pterocarya* and extinct temperate trees

Pterocarya fraxinifolia currently grows from the SW of the Black Sea to the SE of the Caspian Sea in areas with both atmospheric and soil humidity (Browicz and Zielinski, 1982). No pollen of *Pterocarya* is recorded in pollen traps located in Yalova, north of Istanbul and in eastern Thrace (Altunoglu et al., 2008; Karlıoglu et al., 2014, 2015, 2021). It is absent from Holocene diagrams in the SoM (Çaner and Algan, 2002; Valsecchi et al., 2012) and in lakes nearby (Lake Iznik, Miebach et al., 2016; Lake Manyas, Leroy et al., 2002). It is also absent in seven late Pleistocene - Holocene cores of the SoM studied by Mudie et al. (2002, 2007). In the current MIS 5 Marmara sequences, it remains present rather late, i.e. up to Saint-Germain I (roughly equivalent to MIS 5c). The eastern coring site (core CS18) is still nowadays at the border of the *Pterocarya* range in the eastern Marmara region.

However inTenaghi Philippon (Greece) sequence, *Pterocarya* makes its last appearance already at MIS 11, in Valle di Castiglione (Italy) in MIS 7 and in Ohrid (Macedonia/Albania)in MIS 7 too (Tzedakis et al., 2001; Magri et al., 2017; Kousis et al., 2018; Yedema, 2019; Donders et al., 2021). In the S-E Black Sea core reflecting vegetation in northern Anatolia in MIS 5e, some occurrences of *Pterocarya* are observed (Shumilovskikh et al., 2013). It is common in the Georgian Caucasus during the Karagantian Interglacial, equivalent to the Eemian Interglacial, where it still grows nowadays (Shatilova et al., 2011). In the Eemian, it is absent from Ioannina in Greece (Tzedakis et al., 2002) and from the Bulgarian sequence, further north (Bozilova and Djankova, 1976). This extinction gradient, earlier in the west and later in the east, until presence in the southern Black Sea, allows to follow a progressive withdrawal from Europe to the southern Ponto-Caspian region.

Here, pollen from “Tertiary” taxa or, more correctly, from extinct temperate trees that are mostly warm-loving and less drought-intolerant (Svenning, 2003), are largely restricted to the Saalian part of the sequence and are not present in the interstadials and interglacials. They are thus considered as very unlikely to be part of the regional flora at the time (Biltekin et al., 2015). Because of the large number of fungal spores and reworked elements, these taxa are considered as reworked elements. Moreover, these extinct temperate trees are also absent from the Bulgarian site and from the S-E Black Sea core (Bozilova and Djankova, 1976; Shumilovskikh et al., 2013).

The SoM, perhaps due to the close proximity to the Mediterranean vegetation zone, does not appear to be ideal for tree refugia. This can be seen in the maps of potential refugia for warm-loving summer-green trees generated by climate models during the Last Glacial Maximum (Arpe et al., 2011). The closest refugia to the SoM

are in the east of continental Greece (c. 400 km, at Magnesia) and along the south coast of the Black Sea (c. 600 km, at Samsun).

6.6 Palaeoclimatic reconstruction

6.6.1 Climatic patterns for the Marmara region

Based on the taphonomic problems mentioned above, palaeoclimatic reconstructions focus thus only on the depths of 2057 to 1399 cm in core CS22 and 790 and 450 cm in core CS18, roughly MIS 5 (Fig. 6).

The climatic reconstructions for both cores CS22 and CS18 show comparable values along the last interglacial period (Fig. 6). In cores CS22 and CS18, both phases 1 are marked by warm (annual temperature above 10°C) and humid climatic conditions (600 to 800 mm), are very comparable and probably correspond to the Eemian period. A cold event (especially cold summers) is depicted in both sequence (phase 1b).

Later, two cold phases (both summers and winters) are evidenced in core CS22 (phase 2 and 4), corresponding to Melisey I and Melisey II Stadials. Melisey I Stadial shows a long climate period marked by cold and very dry conditions (temperature decreases to 1°C, and precipitations are around 200 mm only) while Melisey II Stadial appears cold and dry but less cold and dry than Melisey I (annual temperature around 6°C and precipitations around 450 mm).

6.6.2 Regional climatic comparison

Climatic changes reconstructed in the SoM are in agreement with the climatic trends that were revealed at Lake Ohrid (Fig. 7). A multi-method approach including the modern analogues technique was applied to the high-resolution pollen sequence

of Lake Ohrid, to provide quantitative estimates of climate during MIS 6 and MIS 5 (Sinopoli et al., 2019).

Cold and dry conditions were reconstructed for the period of 160 – 128 ka ago (i.e. 2nd part of MIS 6, penultimate glacial) in the Balkans from the Lake Ohrid pollen record. Towards the end of the glacial period, the temperatures and precipitation were increasing. This pattern agrees well with the temperature with warming summers and cold winters and dry annual conditions seen in the SoM from the core CS18 from 790 to 730 cm depth (Fig. 6). At Ohrid, the onset of the last interglacial corresponding to the Eemian is abrupt and characterized by humid and warm conditions, with temperatures higher than today (by c. 2 °C) and precipitation 100 mm less precipitation than current (Sinopoli et al., 2019). This pattern is in agreement with the warm and relatively humid conditions reconstructed from cores CS18 and CS22 in the SoM (phase 1).

At Ohrid, a cool and humid event is suggested between 120.3 and 118.5 ka (Sinopoli et al., 2019). This event probably corresponds to the cool/humid event depicted in our Marmara reconstruction (Fig. 6, CS18 and CS22: phase 1b). However, the dinocyst assemblages analyzed in same Marmara cores (Fig. 8) indicate, for this short period, the occurrence of warm-loving dinocyst and seasonal-contrast taxa in surface waters, which diverge to the cold conditions reconstructed here and in Ohrid from pollen assemblages. Other studies have highlighted a cold mid-Eemian period by analysis of biogenic silica and siliceous microfossils in Lake Baikal and elsewhere (Karabanov et al., 2000). With the present chronologies, it is impossible to establish if it is the same event. More temperature reconstructions based on different proxies as chironomids (Plikk et al., 2019), molecular biomarkers

(Hoelworth et al., 2017) or speleothems are required (Drysdale et al., 2005; Regatierri et al., 2017; Wilcox et al., 2020) to corroborate or not this assumption.

As an independent tool, Hoelworth et al. (2017) have used molecular (lipids) biomarkers “TEX 86” to reconstruct the temperature of the surface waters of Lake Ohrid during the MIS 6 and 5. Their results show that the TEX 86 biomarkers reflect the climatic changes during the last glacial-interglacial transition and indicate warm conditions during the Eemian, in agreement with the Ohrid and the Marmara pollen–inferred climate reconstructions.

In order to discuss the Marmara climate signal for the Eemian period at a wider scale, it is compared with the climate patterns inferred from southern European pollen records by Brewer et al. (2008). The latter have reconstructed the climate during the Eemian for central-northern and southern Europe, using a multi-method approach, including the modern analogues technique. Brewer et al. (2008) had identified a climate tri-partition during the Eemian for northern European sites, while in the south, the climate appears to have remained warm with stable conditions. Thus, the Marmara climate reconstruction shows greater similarity with climate patterns inferred from Lake Ohrid than with southern European pollen records ones (Sinopoli et al., 2019), which is probably due to the position of the Marmara sites closer to Lake Ohrid than to other southern sites (Monticchio, Ioannina and two marine cores located in the western Mediterranean Sea). However, this hypothesis needs further testing as very few climate reconstructions are available for southern Europe for this key time period. Eastern sites are still lacking.

Concerning the precipitation signal, humid conditions are reconstructed during the Eemian in the Marmara region (beside dry summers in phase 1a in core CS18). This pattern corroborates the results obtained from the Lake Ohrid pollen sequence,

where precipitation reaches the highest values during the Eemian and decrease until the end of the Eemian at 112 ka (Sinopoli et al., 2019). The humid pattern at Marmara suggests a generally good agreement with the hydrological variations detected in Italy in speleothems (Drysdale et al., 2005; Regattieri et al., 2014, 2017).

Following the Eemian, the early last glacial (from 112 to 70 ka) is characterized in the Marmara cores by a succession of cold and warm periods (Fig. 6, phases 2, 3,4 core CS22) in agreement with the alternation of cold/dry and warm/humid events evidenced at Ohrid (Sinopoli et al., 2019).

7 Comparison of the 2019 chronology and the current chronology

Core CS22 covers a large part of the second half of the Eemian Interglacial with the first part missing (Fig. 7 and 8). This second part of the Eemian Interglacial is interrupted by a continental period. The Eemian Interglacial is followed by the Melisey I Stadial, the Saint-Germain I Interstadial, the Melisey II Stadial and the Saint-Germain II Interstadial (Fig. 7 and 8). In the CS18 sequence, a large portion of the Saalian Glacial (c. MIS 6) is found. It is followed by a rather complete (but not totally complete) Eemian Interglacial, also incorporating a continental phase in its second half. Then the Melisey I Stadial is quasi completely missing, unless the last sample of zone 18P-7 and the first one of zone 18P-8 (lower deciduous *Quercus* percentages) reflect the fringes of this missing stadial (Fig. 7 and 8). The Saint-Germain I Interstadial is identified before the end of MIS 5, suggesting that Melisey II Stadial and Saint-Germain II Interstadial are also missing. Core CS 18 contains thus more significant gaps than core CS22.

Finally, the two sequences complete each other. When taking core CS 22 for the upper part, i.e. Saint-Germain II down to the pine zone in the Eemian, and then core CS18 for the lower part, i.e. the pine zone in the Eemian down to the Saalian Glacial. Thus, a quasi-complete sequence from the Saalian Glacial to Saint-Germain II Interstadial is recorded despite hiati (Fig. 7 and 8).

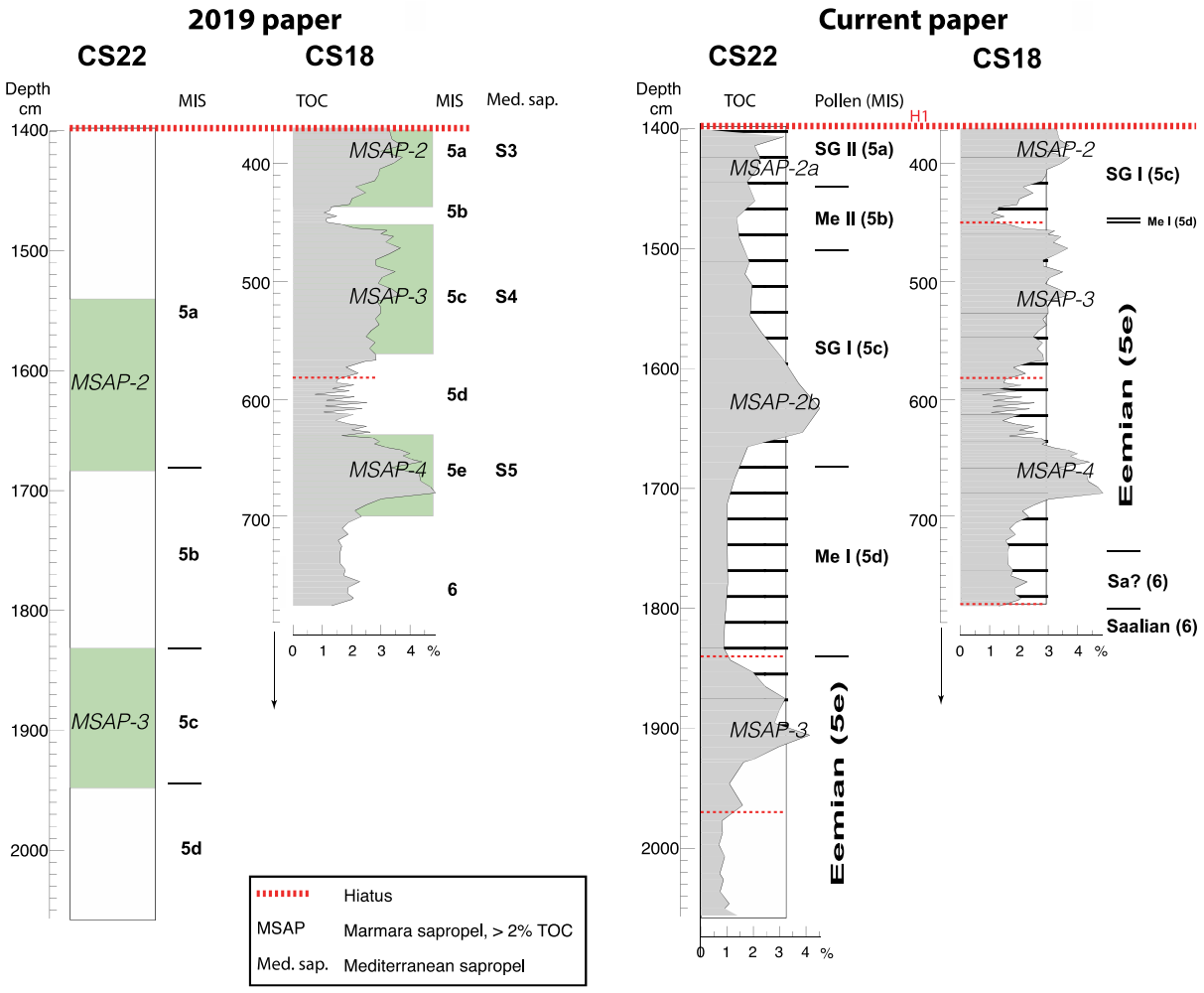

Figure 9: Comparison of the Çağatay et al. (2019) chronology and the present chronology. TOC = Total Organic Carbon, MIS = Marine Isotopic Stage, Me I = Melisey I Stadial, SG I = Saint-Germain I Interstadial, Me II = Melisey II Stadial, SG II = Saint-Germain II Interstadial, Saal = Saalian Glacial.

Significant differences with the chronology proposed by Çağatay et al. (2019) were found (Fig. 9; Table 1). In the current paper, palynological analyses of the two cores (pollen and dinocysts) are a new feature. Moreover, the TOC and the Ca values of core CS22 from Kende (2018) are provided in the current paper and could not be included in the Çağatay et al. (2019) paper yet.

Table 1: Summary of the arguments for the two chronologies: Çağatay et al. (2019) chronology and the present chronology

1 New data
a. Pollen zones 18P-3 to 5 belong to the Eemian Interglacial as shown by the similarity of reconstructed vegetation (especially Mediterranean taxa) and reconstructed palaeoclimate (especially warmer annual temperatures) to the Eemian Interglacial of the Tenaghi Philippon and Ohrid sequences. The zones identified as belonging to the Eemian also display the occurrence of warm—loving dinocysts.
b. Strong similarities exist between the *Pinus* zone 22P-2 and *Pinus* zone 18P-6, as well as between the end of the marine phases (as per dinocyst data) in the cores CP22 and CP18.
c. These two *Pinus* zones are not stadials, as not dry and cold; but they are humid and cold fluctuations within the Eemian Interglacial on the base of the occurrence of high values of *Abies* and deciduous *Quercus* and reconstructed palaeoclimate.
d. The three sapropels formed during interstadials (pollen analysis) but under three different surface water conditions (dinocyst analysis): marine, marine to lacustrine and lacustrine.

e. Just below the red-H1 seismic marker, maximal values of Ca at 1450-1400 cm in core CS22 are missing in cores CS18 and CS27. Possibly the Ca peak at 1575-1510 cm in core CS22 is missing in the two other cores too.
2 Change of emphasis The red-H1 seismic reflector is a major erosion horizon at the seismic scale, much larger than other erosion levels identified further down the cores, and thus probably much longer. It has been correctly identified in the three cores because of its outstanding reflectivity and lithology.
3 Change in reasoning Based on the parsimony principle and starting at the base with the Eemian interglacial, the successive stadials and interstadials are progressively identified upwards, leaving thus the largest gap below the major erosion level, comprised by the red-H1 reflector.

In consequence, the following main differences are found (Fig. 9). In core CS18, the absence of Saint-Germain II Interstadial (MIS 5a) and Melisey II Stadial (MIS 5b) and possibly the occurrence of only a much-reduced Melisey I Stadial (MIS 5d) are noted. The sequence of core CS22 extends to the Eemian Interglacial (MIS 5e) instead of Melisey I Stadial only (MIS 5d).

8 Conclusions

Even if containing some hiatus largely covered by splicing the two long sequences, the results of this new pollen investigation in the SoM are a significant contribution, because of the scarcity of pollen records in the eastern Mediterranean region at large for the last interglacial and two subsequent interstadials as well as for the previous glacial. Moreover, the current study is the only one combining terrestrial (pollen) and marine (dinocysts) signals in the same cores for this period.

No absolute dates are available, but the proposed chronology in the current state of the art is more detailed than that previously published as it is based on more information: inter-core correlations based on some new geochemical indicators, recognition of basin-wide hiati, and the possibility of correlation to the European stratigraphy, especially owing to the recognition of the characteristics of the Eemian, a milestone in palynostratigraphy. It allows obtaining a nearly complete record from the Saalian Glacial to the Saint-Germain II Interstadial. It is also confirmed that the sapropels formed during warm climatic conditions only.

A later occurrence of *Pterocarya,* i.e. up to Saint-Germain I Interstadial, is established in the Marmara sequences in comparison to the other pollen records of the Valle di Castiglione, Ohrid, Ioannina and Tenaghi Philippon sequences, and in agreement with the current distribution of *Pterocarya* in the Black Sea region.

The Saalian Glacial is in two parts, a forest-steppe with a strongly erosive environment followed by a drier *Artemisia* steppe. A clear development of Mediterranean taxa was observed in the Eemian Interglacial especially in the eastern core, supporting the results of the pollen reconstruction from L. Ohrid: warmer than present and possibly drier at its peak. For the rest of the interglacial period, warm and humid conditions are reconstructed from cores CS18 and CS22 in the SoM, interrupted by cold and dry climate periods corresponding to Melisey I and II Stadials. The Marmara climatic reconstruction shows greater similarity with climatic patterns inferred from Lake Ohrid than with southern European pollen records ones (Monticchio and Ioannina).

At the peak of the Eemian, the Marmara region, instead of being in the steep climatic gradient between the Euxinian and the Mediterranean ecosystems, falls clearly in the Mediterranean ecosystem due to a shift of the Mediterranean climate

northeastwards. The MIS 11 (Holsteinian Interglacial) has a closer insolation configuration to that of the Holocene one than the Eemian one (Candy et al., 2014; Bolikhovskaya and Molodkov, 2018). It would represent a good target for subsequent investigations. Additionally, it may reasonably be forecasted that, with the Anthropocene, the Euxinian ecosystem will be further reduced and that a Mediterranean climate will prevail in the whole Marmara region.

Data availability

The pollen data have been contributed to the European Pollen Database.

Acknowledgements

Cores were taken during the MARSITECRUISE of Ifremer/Genavir R.V. Pourquoi Pas?, within the framework of MARSITE FP7 EU Project (grant agreement no: 308417). We are grateful to the University of Liverpool (UK) and IMBE (France) pollen laboratories for pollen extraction and to M. Garcia-Molina from the Inorganic Geochemistry Unit of the CEREGE (France) for the ITRAX-ICPMS measurements. Thanks are due to N. Çağatay, K. Eriş and N. Yakupoğlu from ITU (Turkey) who gave access to core CS18 for sampling and contributed to the improvement of this publication owing to inspiring discussions over the years, especially on the chronology.

G. Sinopoli, L. Sadori and A.M. Mercuri to have made the pollen data (MIS 5) of Lake Ohrid available. Part of this work has been supported by Bilateral ANR/TÜBITAK collaborative research project MAREGAMI (ANR-16-CE03-0010-02) and Tubitak Project (116Y371). This paper is an ISEM contribution N°XXXX.

We are grateful to the reviewers for their comments.

References

Altunoglu, M.K., Bikakci, A., Celenk, S., Canitez, Y., Malyer, H., Sapan, N., 2008 Airborne pollen grains in Yalova, Turkey, 2004. Biologia 63, 5, 658—663.

Arpe, K., Leroy, S.A.G., Mikolajewicz, U., 2011. A comparison of climate simulations for the last glacial maximum with three different versions of the ECHAM model and implications for summer-green tree refugia. Climate of the Past 7, 91–114.

Atalay, I., Efe, R., 2010. Structural and distributional evaluation of forest ecosystems in Turkey. Journal of Environmental Biology 31, 61-70.

Aydoğdu, A., Pinardi, N., Özsoy, E., Danabasoglu, G., Gürses, O, Karspeck, A., 2018. Circulation of the Turkish Straits System under interannual atmospheric forcing. Ocean Sci. 14, 999–1019.

Bennett, K., 2007. Psimpoll and Pscomb Programs for Plotting and Analysis. Version Psimpoll 4.27. http://chrono.qub.ac.uk/psimpoll/psimpoll.html (accessed 27 May 2020).

Beşiktepe, S.T., Sur, H.I., Özsoy, E., Latif, M.A., Oğuz, T., Ünlüata, Ü., 1994. The circulation and hydrography of the Marmara Sea. Prog. Oceanogr. 34, 285–334.

Beug, H.-J., 1967. Contribution to the postglacial vegetational history of northern Turkey. in: Cushing, E., Wright, H. (Eds), Quaternary Palaeoecology. Yale University Press, New Haven, CT, pp. 349-356.

Beug, H.-J., 2004. Leitfaden der Pollenbestimmung für Mitteleuropa und angrenzende Gebiete: Mit 736 13 Tabellen. Pfeil, München.

Biltekin, D., Popescu, S.-M., Suc, J.-P., Quézel, P., Jiménez-Moreno, G., Nurdan Yavuz, N., Çağatay, M.N., 2015. Anatolia: A long-time plant refuge area documented by pollen records over the last 23 million years. Review of Palaeobotany and Palynology 215, 1–22.

Bolikhovskaya, N. S., Molodkov, A.N., 2018. Study of cyclicity in the evolution of vegetation and climate of the Neopleistocene for searching of palaeoenvironmental analogue of the Holocene. Practical Geography and XXI Century Challenges: The 2018 IGU Thematic Conference dedicated to the centennial of the Institute of Geography of Russian Academy of Sciences. Conference Book. Part 1. Moscow: Institute of Geography, Russian Academy of Sciences, pp. 158-166.

Božilova, E., Djankova, M., 1976. Vegetation development during the Eemian in the North Black Sea Region. Phytology 4, 25–32.

Brauer, A., Allen, J.R.M., Mingram, J., Dulski, P., Wulff, S., Huntley, B., 2007 Evidence for last interglacial chronology and environmental change from Southern Europe. PNAS 104, 2, 450–455.

Brewer, S., Guiot, J., Sanchez-Goñi, M.F., Klotz, S., 2008. The climate in Europe during the Eemian: a multi-method approach using pollen data. Quat. Sci. Rev. 27, 2303-2315. https://doi.org/10.1016/j.quascirev.2008.08.029.

Browicz, K., 1989. Chrorology of the Euxinian and Hyrcanian element in the woody flora of Asia. Plant Systematics and Evolution 162, ¼, 305-314.

Browicz, K., Zielinski, J., 1982. Chronology of trees and shrubs in south-west Asia and adjacent regions. Polish Scientific Publishers, Warsaw, Poland.

Çağatay, M.N., Eriş, K., Ryan, W.B.F., Sancar, Ü., Polonia, A., Akçer, S., Biltekin, D., Gasperini, L., Görür, N., Lericolais, G., Bard, E., 2009. Late Pleistocene–Holocene evolution of the northern shelf of the Sea of Marmara. Marine Geology 265, 87–100.

Çağatay, M.N., Eriş K.K., Makaroglu Ö., Yakuboğlu N., Henry P., Leroy S., Uçarkuş G., Sakınç M., Yalamaz B., Bozyiğit C., Kende J., 2019. The Sea of Marmara during Marine Isotope Stages 5 and 6. Quat Sc Rev 220, 124-141.

Candy, I., Schreve, D.C., Sherriff, J., Tye, G.J., 2014. Marine Isotope Stage 11: Palaeoclimates, palaeoenvironments and its role as an analogue for the current interglacial. Earth-Science Reviews, 128,18-51.

Çaner, H., Algan, O., 2002. Palynology of sapropelic layers from the Marmara Sea. Marine Geology 190, 35-46.

Cheddadi, R., Mamakowa, K., Guiot, G., De Beaulieu J.L., Reille, M., Granoszewski W., Peyron, O., 1998. Was the climate of the Eemian stable? A quantitative climate reconstruction from seven European pollen records. Palaeogeography, Palaeoclimatology, Palaeoecology, 143, 73-85.

Cheddadi, R., Rossignol-Strick, M., 1995. Improved preservation of organic matter and pollen in eastern Mediterranean sapropels. Paleoceanography 10, 2, 301-309.

Chen, C., Litt, T., 2018. Dead Sea pollen provides new insights into the paleoenvironment of the southern Levant during MIS 6-5. Quaternary Science Reviews 188, 15-27.

Chepalyga, A.L., 2007. The late glacial great flood in the Ponto-Caspian basin. in: Yanko-Hombach, V., Gilbert, A.S., Panin, N., Dolukhanov, P.M. (Eds), The Black Sea Flood Question. Springer, pp. 119-148

Chevalier, M., Davis, B.A.S., Heiri, O., Seppä, H., Chase, B.M., Gajewski, K., Lacourse, T., Telford, R.J., Finsinger, W., Guiot, J., Kühl, N., Maezumi, S.Y., Tipton, J.R., Carter, V.A., Brussel, T., Phelps, L.N., Dawson, A., Zanon, M., Vall□e, F., Nolan, C., Mauri, A., de Vernal, A., Izumi, K., Holmstrom, L., Marsicek,

J., Goring, S., Sommer, P.S., Chaput, M., Kupriyanov, D., 2020. Pollen-based climate reconstruction techniques for late Quaternary studies. Earth Sci. Rev. 210, 103384. https://doi.org/10.1016/j.earscirev.2020.103384.

Donders, T., Panagiotopoulos, K., Koutsodendris, A., Bertini, A., Mercuri, A.M., Masi, A., Combourieu-Nebout, N., Joannin, S., Kouli, K., Kousis, I., Peyron, O., Torri, P., Francke, A., Wagner, B., Sadori, L., 2021. 1.36 million years of Mediterranean forest refugium dynamics in response to glacial-interglacial cycle strength. PNAS, 118 (34) e2026111118; https://doi.org/10.1073/pnas.2026111118.

Dugerdil, L., Joannin, S., Peyron, O., Jouffroy-Bapicot, I., Vanniere, B., Bazartseren, B., Unkelbach, J., Behling, H., Menot, G., 2021. Climate reconstructions based on GDGT and pollen surface datasets from Mongolia and Siberia: calibrations and applicability to extremely cold-dry environments over the Late Holocene. Clim. Past 17, 1199–1226, https://doi.org/10.5194/cp-17-1199-2021.

Felde, V. A., Flantua, S.G.A., Jenks, C.R., Benito, B.M., de Beaulieu, J.-L. et al.. 2020. Compositional turnover and variation in Eemian pollen sequences in Europe. Vegetation History and Archaeobotany, Springer Verlag 29 (1), 101-109. 10.1007/s00334-019-00726-5.hal-02091016

Fischer, H., Meissner, K.J., Mix, A.C. et al., 2018. Palaeoclimate constraints on the impact of 2 °C anthropogenic warming and beyond. Nature Geosci 11, 474–485. https://doi.org/10.1038/s41561-018-0146-0

Francke, A., Wagner, B., Just, J., Leicher, N., Gromig, R., Baumgarten, H., Vogel, H., Lacey, J. H., Sadori, L., Wonik, T., Leng, M. J., Zanchetta, G., Sulpizio, R., Giaccio, B., 2016. Sedimentological processes and environmental variability at Lake Ohrid (Macedonia, Albania) between 637 ka and the present, Biogeosciences 13, 1179–1196, https://doi.org/10.5194/bg-13-1179-2016.

Gökaşan, E., Ergin, M., Özyalvaç, M., Sur, H.I., Tur, H., Görüm, T., Ustaömer, T., Batuk, F.G., Alp, H., Birkan, H., Türker, A., Gezgin, E., Özturan,M., 2008. Factors controlling the morphological evolution of the Çanakkale Strait (Dardanelles, Turkey). Geo-Mar. Lett. 28,107–129.

Grall, C., Henry, P., Thomas, Y., Westbrook, G.K., Çağatay, M.N., Marsset, B., Géli, L., 2013. Slip rate estimation along the western segment of the Main Marmara Fault over the last 405-490 ka by correlating mass transport deposits. Tectonics 32, 6, 1587-1601.

Grall, C., Henry, P., Westbrook, G.K., Çağatay, M.N., Thomas, Y., Marsset, B., Borschneck, D., Saritas, H., Cifçi, G., Géli, L., 2014. Mass Transport Deposits Periodicity Related to Glacial Cycles and Marine-Lacustrine Transitions on a Ponded Basin of the Sea of Marmara (Turkey) Over the Last 500 ka. In: Krastel, S. et al. (Eds.), Submarine Mass Movements and Their Consequences, Advances in Natural and Technological Hazards Research 37, Springer International Publishing Switzerland, 595-603.

Guiot, J., 1990. Methodology of the last climatic cycle reconstruction in France from pollen data. Palaeogeogr. Palaeoclimatol. Palaeoecol. 80, 49-69.

Henry, P., Kende J., 2015. MARSITECRUISE R/V Pourquoi pas? October 28th – November 17th, 2014. Leg 3 - Six-Month Cruise Report. https://doi.org/10.13155/54534

Holtvoeth, J., Vogel, H., Valsecchi, V., Lindhorst, K., Schouten, S., Wagner, B., Wolff, G. A., 2017. Linear and non-linear responses of vegetation and soils to glacial-interglacial climate change in a Mediterranean refuge. Sci Rep 7, 8121. https://doi.org/10.1038/s41598-017-08101-yJuggins and Juggins, 2019

Hooghiemstra, H., Lézine, A.-M., Leroy, S.A.G., Dupont, L., Marret, F., 2006. Late Quaternary palynology in marine sediments: a synthesis of the understanding of pollen distribution patterns in the NW African setting. Quaternary International, 148, 29-44.

Kazancı, N., Leroy, S., Ileri, Ö., Emre, O., Kibar, M., Öncel, S., 2004. Late Holocene erosion in NW Anatolia from sediments of Lake Manyas, Lake Ulubat and the southern shelf of the Marmara Sea, Turkey. Catena 57, 277-308.

Karlıoğlu, N., Çaner, H., Akkemik, U., 2014. Modern pollen distribution at Iğneada waterlogged forests between the periods September 2007 – August 2009. Eurasian Journal of Forest Science 2, 2, 7-17.

Karlıoğlu, N., Çaner, H., Akkemik, U., Köse, N., Kindap, T., 2015. Modern pollen monitoring of native trees in Belgrad forest, Istanbul (northwestern Turkey). Comptes rendus de l'Académie bulgare des Sciences 68, 1, 39-48.

Karlıoğlu, N., Çaner, H., Akkemik, U, Filipova-Marinova, E., 2021. Two-year record of pollen monitoring in *Fagus orientalis* forest (NW Turkey). Comptes rendus de l'Académie bulgare des Sciences 74, 3, 379-388.

Kende, J., 2018. Tectonique et hydrologie en mer de Marmara : Histoire de l'ouverture de la mer de Marmara et reconstitution de la réponse hydrologique aux variations climatiques depuis le dernier interglaciaire. Thèse de doctorat, Aix-Marseille Université. 18 pp. https://hal.science/tel-01907260v1/document

Koreneva, E.V., Kartashova, G.G., 1978. Palynological study of samples from holes 379A, 380A, LEG 42B. in: Ross, D.A., Neprochnov, Y.P. (Eds.), Initial Reports of the Deep Sea Drilling Project. U.S. Government Printing Office, Washington, pp. 951–992.

Kotthoff U., Pross J., Müller U. C., Peyron O., Schmiedl G., Schulz H., Bordon A., 2008. Climate dynamics in the borderlands of the Aegean Sea during formation of sapropel S1 deduced from a marine pollen record. Quaternary Science Reviews 27, 832–845.

Kousis I., Koutsodendris A., Peyron O., Leicher N., Francke A., Wagner B., Giaccio B., Knipping M., Pross J., 2018. Centennial-scale vegetation dynamics and climate variability in SE Europe during Marine Isotope Stage 11 based on a pollen record from Lake Ohrid. Quaternary Science Reviews 190, 20-38.

Kutiel, H., Türkes, M., 2017. Spatial and temporal variability of dryness characteristics in Turkey. Int. J. Climatol. 13, S1,818-828.

Leroy, S.A.G., 2010. Sea level and palaeoclimatic changes in the south and middle Caspian Sea region since the Lateglacial from palynological analyses of marine sediment cores. Geography, Environment, Sustainability, Faculty of Geography of Lomonosov Moscow State University and by the Institute of Geography of RAS. 2, 32-41. http://www.geogr.msu.ru/GESJournal/,

Leroy, S.A.G., Giralt, S., Francus, P., Seret, G., 1996. The high sensitivity of the palynological record in the Vico maar lacustrine sequence (Latium, Italy) highlights the climatic gradient through Europe for the last 90 ka. Quat. Sc. Rev. 16, 2-3, 189-201.

Leroy, S., Kazancı, N., Ileri, Ö., Kibar, M., Emre, O., McGee, E., Griffiths, H. I., 2002. Abrupt environmental changes within a late Holocene lacustrine sequence south of the Marmara Sea (Lake Manyas, N-W Turkey): possible links with seismic events. Marine Geology 190, 1-2: 531-552.

Leroy, S.A.G., Arpe, K., Mikolajewicz, U., 2011. Vegetation context and climatic limits of the Early Pleistocene hominin dispersal in Europe. Quat. Sci. Rev. 30, 1448-1463.

Leroy, S.A.G., López-Merino, L., Tudryn, A., Chalié, F., Gasse, F., 2014. Late Pleistocene and Holocene palaeoenvironments in and around the Middle Caspian Basin as reconstructed from a deep-sea core. Quaternary Science Reviews 101, 91-110. DOI 10.1016/j.quascirev.2014.07.011

Leroy, S.A.G., Lahijani, H., Crétaux, J.-F., Aladin, N., Plotnikov, I., 2020. Past and current changes in the largest lake of the world: The Caspian Sea. in: Mischke, S. (Ed.), Large Asian lakes in a changing world. Springer, pp. 65-107.

Leroy, S.A.G., Henry, P., Marret, F., Pailles, C., Licari, L., Kende, J., Rostek, F., Bard, E., accepted. Dinocyst assemblages and water surface conditions in the Sea of Marmara during MIS 6 and 5 from two long cores. Quaternary Science Reviews

Lézine, A.-M., von Grafenstein, U., Andersen, N., Belmecheri, S., Bordon, A., Caron, B., Cazet, J.-P., Erlenkeuser, H., Fouache, E., Grenier, C., Huntsman-Mapila, P., Hureau-Mazaudier, D., Manelli, D., Mazaud, A., Robert, C., Sulpizio, R., Tiercelin, J.-J., Zanchetta, G., Zeqollari, Z., 2010. Lake Ohrid, Albania, provides an exceptional multi-proxy record of environmental changes during the last glacial–interglacial cycle. Palaeogeography, Palaeoclimatology, Palaeoecology 287, 116–127.

Lisiecki, L.E., Raymo, M.E., 2005. A Pliocene-Pleistocene stack of 57 globally distributed benthic d18O records. Paleoceanography, 20, PA1003

Magri, D., Di Rita, F., Aranbarri, J., Fletcher, W., González-Sampériz, P., 2017. Quaternary disappearance of tree taxa from Southern Europe: Timing and trends. Quaternary Science Reviews 163, 23-55

Marinova, E., Harrison, S., Bragg, F., Connor, S., de Laet, V., Leroy, S.A.G., Mudie, P. and 18 co-authors, 2018. Pollen-derived biomes in the Eastern-Mediterranean-Black Sea-Caspian corridor. Journal of Biogeography 45, 2, 484-499. DOI: 10.1111/jbi.13128

Miebach, A., Niestrath, P., Roeser, P., Litt, T., 2016. Impacts of climate and humans on the vegetation in northwestern Turkey: palynological insights from Lake Iznik since the Last Glacial. Clim. Past 12, 575–593.

Milner, A.M., Müller, U.C., Roucoux, K.H., Collier, R.E.L., Pross, J., Kalaitzidis, S., Christanis, K., Tzedakis, P.C., 2013. Environmental variability during the Last Interglacial: A new high-resolution pollen record from Tenaghi Philippon, Greece. Journal of Quaternary Science 28, 113-117.

Milner, A.M., Roucoux, K.H., Collier, R.E.L., Müller, U.C., Pross, J., Tzedakis, P.C. 2016. Vegetation responses to abrupt climatic changes during the Last Interglacial Complex (Marine Isotope Stage 5) at Tenaghi Philippon, NE Greece. Quaternary Science Reviews 154, 169-181.

Mudie, P.J., Rochon, A., Aksu, A.E., 2002. Pollen stratigraphy of Late Quaternary cores from Marmara Sea: land–sea correlation and paleoclimatic history. Marine Geology 190, 233–260.

Mudie, P.J., Marret, F., Aksu, A.E., Hiscott, R.N., Gillespie, H., 2007. Palynological evidence for climatic change, anthropogenic activity and outflow of Black Sea water during the late Pleistocene and Holocene: Centennial- to decadal-scale

records from the Black and Marmara Seas. Quaternary International 167–168, 73–90.

Mudie, P.J., Leroy, S.A.G., Marret, F., Gerasimenko, N., Kholeif, S.E.A., Sapelko, T., Filipova-Marinova, M., 2011. Non-Pollen Palynomorphs: Indicators of Salinity and Environmental Change in the Caspian-Black Sea-Mediterranean Corridor. in: Buynevich, I., Yanko-Hombach, V., Gilbert, A.S., Martin, R.E. (Eds), Geology and Geoarchaeology of the Black Sea Region: Beyond the Flood Hypothesis. Geological Society of America Special Paper 473, pp. 89–115.

Müller, U., Pross, J., Tzedakis, P.C., Gamble, C., Kotthoff, U., Schmiedl, G., Wulf, S., Christanis, K. 2011. The role of climate in the spread of modern humans into Europe. Quaternary Science Reviews 30, 273-279.

Nielsen, R., Akey, J.M., Jakobsson, M., Pritchard, J.K., Tishkoff, S., Willerslev, E. 2017. Tracing the peopling of the world through genomics. Nature 541, 302-310.

North Greenland Ice Core Project members, 2004. High-resolution record of Northern Hemisphere climate extending into the last interglacial period. Nature 431, 7005, 147-151, 9 September 2004

Okay, S., Sorlien, C., Cormier, M.-H., Barin, B., Seeber, L., Çifçi, G., Dondurur, D., Kurt, H, Küçük, H.M., Atgin, O., Özel, Ö., 2022. Post-500 ka and Holocene activity on distributed faults of the North Anatolian Fault system along the southern shelf of Marmara Sea, Turkey. Tectonophysics 229547.

Ön, Z.B., Özeren, M.S., 2019. Temperature and precipitation variability in eastern Anatolia: Results from independent component analysis of Lake Van sediment data spanning the last 250 kyr BP, Quaternary International 514, 119-129

Peyron, O., Magny, M., Goring, S., Joannin, S., de Beaulieu, J.-L., Brugiapaglia, E., Sadori, L., Garfi, G., Kouli, K., Ioakim, C., Combourieu-Nebout, N., 2013.

Contrasting patterns of climatic changes during the Holocene across the Italian Peninsula reconstructed from pollen data. Clim. Past 9, 1233-1252. https://doi.org/10.5194/cp-9-1233-2013.

Peyron, O., Combourieu-Nebout, N., Brayshaw, D., Goring, S., Andrieu-Ponel, V., Desprat, S., Fletcher, W., Gambin, B., Ioakim, C., Joannin, S., Kotthoff, U., Kouli, K., Montade, V., Pross, J., Sadori, L., Magny, M., 2017. Precipitation changes in the Mediterranean basin during the Holocene from terrestrial and marine pollen records: a modeledata comparison. Clim. Past 13, 249-265. https://doi.org/ 10.5194/cp-13-249-2017.

Pickarski, N., Kwiecien, O., Djamali, M., Litt, T., 2015. Vegetation and environmental changes during the last inter-glacial in eastern Anatolia (Turkey): a new high-resolution pollen record from Lake Van. Palaeogeogr. Palaeocl. Palaeoecol. 145-158, https://doi.org/10.1016/j.palaeo.2015.06.015,

Pickarski, N., Litt, T., 2017. A new high-resolution pollen sequence at Lake Van, Turkey: insights into penultimate interglacial–glacial climate change on vegetation history. Clim. Past, 13, 68-710.

Poliak, V.J., et al., 2018. A highly resolved record of relative sea level in the western Mediterranean Sea during the last interglacial period. Nature Geoscience 11, 860–864.

Reille, M., 1992. Pollen et spores d'Europe et d'Afrique du nord: Laboratoire de botanique historique et palynologie. URA CNRS, Marseille, France.

Reille, M., 1995. Pollen et spores d'Europe et d'Afrique du Nord. Supplément 1. Laboratoire de Botanique historique et Palynologie: Marseille. 543 pp.

Reille, M., 1998. *Pollen et spores d'Europe et d'Afrique du Nord, Supplément 2* . Éditions du Laboratoire de botanique historique et palynologie, Marseille, 530 p.

Robles, M., Peyron, O., Brugiapaglia, E., Ménot, G., Dugerdil, L., Ollivier, V., Ansanay-Alex, S., Develle, A.-L., Tozalakyan, P., Meliksetian, K., Sahakyan, K., Sahakyan, L., Perello, B., Badalyan, R., Colombié, C., Joannin, S., 2022. Impact of climate changes on vegetation and human societies during the Holocene in the South Caucasus (Vanevan, Armenia): a multiproxy approach including pollen, NPPs and brGDGTs. Quaternary Science Reviews 277, 107297

Roucoux, K.H., Tzedakis, P.C., Lawson, I.T., Margari, V. 2011. Vegetation history of the penultimate glacial period (Marine Isotope Stage 6) at Ioannina, north-west Greece, J. Quaternary Sci., 26, 616–626.

Sadori, L., Koutsodendris, A., Panagiotopoulos, K., Masi, A., Bertini, A., Combourieu-Nebout, N., Francke, A., Kouli, K., Joannin, S., Mercuri, A. M., Peyron, O., Torri, P., Wagner, B., Zanchetta, G., Sinopoli, G., Donders, T. H. 2016. Pollen-based paleoenvironmental and paleoclimatic change at Lake Ohrid (south-eastern Europe) during the past 500 ka. Biogeosciences 13, 1423–1437, https://doi.org/10.5194/bg-13-1423-2016.

Salonen, J.S., Helmens, K.F., Brendryen, J. Kuosmanen, N., Väliranta, M., Goring, S., Korpela, M., Kylander, M., Philip, A., Plikk, A., Renssen, H., Luoto, M., 2018. Abrupt high-latitude climate events and decoupled seasonal trends during the Eemian. Nat Commun 9, 2851. https://doi.org/10.1038/s41467-018-05314-1

Salonen, J.S., Korpela, M., Williams, J.W., Luoto, M., 2019. Machine-learning based reconstructions of primary and secondary climate variables from North American and European fossil pollen data. Sci. Rep. 9, 1-13.

Sánchez-Goñi, M.F., Loutre, M.F., Crucifix M., Peyron, O., Santos, L., Duprat, J., Turon, J.-L., Peypouquet, J.-P., 2005. Increasing vegetation and climate

gradient in Western Europe over the Last Glacial Inception (122-110 ka): models-data comparison. Earth Planet. Sci. Lett. 231, 1-2, 111-130.

Shackleton, N.J., Sanchez-Goñi, M F, Pailler, D., Lancelot, Y., 2003. Marine Isotope Substage 5e and the Eemian Interglacial. Global and Planetary Change 36, 151-155.

Shatilova, I., Mchedlishvili, N., Rukhadze, L., Kvavadze, E., 2011. The history of the flora and vegetation of Georgia (South Caucasus). Georgian National Museum. Tbilisi. 200 pp.

Shumilovskikh, L.S., Arz, H. W, Wegwerth, A., Fleitmann, D., Marret, F., Nowaczyk, N., Tarasov, P., Behling, H., 2013. Vegetation and environmental changes in Northern Anatolia between 134 and 119 ka recorded in Black Sea sediments. Quaternary Research 80, 349–360.

Sinopoli, G., Masi, A., Regattieri, E., Wagner, B., Francke, A., Peyron, O., Sadori, L., 2018. Palynology of the Last Interglacial Complex at Lake Ohrid: palaeoenvironmental and palaeoclimatic inferences. Quat. Sci. Rev. 180, 177-192.

Sinopoli, G., Peyron, O., Masi, A., Holtvoeth, J., Francke, A., Wagner, B., Sadori, L., 2019. Pollen-based temperature and precipitation changes in the Ohrid Basin (western Balkans) between 160 and 70 ka. Clim. Past 15, 53–71.

Sorlien, C.C., Akhun, S.D., Seeber, L., Steckler, M.S., Shillington, D.J., Kurt, H., Imren, C., 2012. Uniform basin growth over the last 500 ka, north Anatolian fault, Marmara Sea, Turkey. Tectonophysics 518, 1-16.

Sun, X., Li, X., Beug, H.-J., 1999. Pollen distribution in hemipelagic surface sediments of the South China Sea and its relation to modern vegetation distribution. Marine Geology 156, 211-226.

Svenning, J.-C., 2003. Deterministic Plio-Pleistocene extinctions in the European cool-temperate tree flora. Ecology Letters 6, 646–653.

Tudryn, A., Leroy, S. A.G., Toucanne, S., Gibert-Brunet, E., Tucholka, P., Lavrushin, Y.A., Dufaure, O., Miska, S., Bayon, G., 2016. The Ponto-Caspian basin as a final trap for southeastern Scandinavian ice-sheet meltwater. Quat. Sci. Rev. 148, 29-43.

Tzedakis, P.C., Andrieu, V., de Beaulieu, J.-L., Birks, H.J.B., Crowhurst, S., Follieri, M., Hooghiemstra, H., Magri, D., Reille, M., Sadori, L., Shackleton, N.J., Wijmstra, T.A., 2001. Establishing a terrestrial chronological framework as a basis for biostratigraphical comparisons. Quat. Sc. Rev. 20, 1583–1592.

Tzedakis, P.C., Lawson, I.T., Frogley, M.R., Hewitt, G.M., Preece, R.C., 2002. Buffered tree population changes in a Quaternary refugium: evolutionary implications. Science 297, 2044-2047.

Unal, Y., Kindap, T., Karaca, M., 2003. Redefining the climate zones of Turkey using cluster analysis. Int. J. Climatol. 23, 1045–1055.

Valsecchi, V., Sanchez Goñi, M. F., Londeix, L., 2012. Vegetation dynamics in the Northeastern Mediterranean region during the past 23 000 yr: insights from a new pollen record from the Sea of Marmara. Clim. Past 8, 1941–1956.

van Geel, B., Aptroot, A., 2006. Fossil ascomycetes in Quaternary deposits. Nova Hedwigia 82, 3-4, 313-329.

Vidal, L., Ménot, G., Joly, C., Bruneton, H., Rostek, F., Çağatay, M.N., Major, C., Bard, E., 2010. Hydrology in the Sea of Marmara during the last 23 ka: Implications for timing of Black Sea connections and sapropel deposition. Paleoceanography 25, PA1205.

Wagner, B., H. Vogel, A. Francke, T. Friedrich, T. Donders, J. Lacey, M. Leng, E. Regattieri, L. Sadori, T. Wilke, G. Zanchetta, C. Albrecht, A. Bertini, N. Combourieu-Nebout, A. Cvetkoska, B. Giaccio, A. Grazhdani, T. Hauffe, J. Holtvoeth, S. Joannin, E. Jovanovska, J. Just, K. Kouli, I. Kousis, A. Koutsodendris, S. Krastel, M. Lagos, N. Leicher, Z. Levkov, K. Lindhorst, A. Masi, M. Melles, A.M. Mercuri, S. Nomade, N. Nowaczyk, K. Panagiotopoulos, O. Peyron, J. Reed, L. Sagnotti, G. Sinopoli, B. Stelbrink, R. Sulpizio, A. Timmermann, S. Tofilovska, P., Torri, F., Wagner-Cremer, T., Wonik, X. Zhang, 2019. Mediterranean winter rainfall in phase with African monsoons during the past 1.36 million years. Nature 573, 256-260. DOI: 10.1038/s41586-019-1529-0

Wijmstra, T.A., Smit, A., 1976. Palynology of the Middle part (30-78 metres) of the 120 m deep section in Northern Greece (Macedonia). Acta. Bot. Neerl. 25, 4, 297-312.

Yaltirak, C., 2002. Tectonic evolution of the Marmara Sea and its surroundings. Marine Geology 190, 493-529.

Yedema, Y., 2019. Paleoenvironmental variations inferred from a high resolution pollen record of MIS 9-10 at ancient Lake Ohrid, North Macedonia. Master thesis, Earth, Life and Climate, Utrecht University, pp. 34.

Zohary, M., 1973. Geobotanical Foundations of the Middle East. G. Fisher Verlag, Stuttgart.

Zumbühl, A., 2010. History of the Black Sea recorded in stalagmites from Northern Turkey. Master's Thesis, Faculty of Science, University of Bern, pp. 115.

Supplementary information

Supplementary information SI1: Dinocyst taxon lists with general affinities

1 Brackish

Pyxidinopsis psilata,

Spiniferites cruciformis/Galeacysta etrusca,

Galeacysta etrusca,

S. cruciformis A,

S. cruciformis B,

S. cruciformis C,

Pterocysta cruciformis,

S. inaequalis,

Romanodinium areolatum,

Caspidinium rugosum,

C. rugosum rugosum,

Impagidinium sp. A,

I. caspienense

2 *Lingulodinium machaerophorum*

Various forms

3 Heterotrophs

Dubridinium caperatum,

Lejeunecysta marieae,

Votadinium calvum,

Brown baggy cyst,

Xandarodinium xanthum,

C. Protoperidinium nudum,

C. Protoperidinium stellatum,

C. Polykrikos hartmanii

4 Marine

S. belerius,

S. bentorii,

S. elongatus,

S. hainanensis,

S. ramosus,

S. septentrionalis,

Spiniferites sp.,

S. mirabilis,

S. pachydermus,

Polysphaeridium zoharyi,

Tuberculodinium vancampoae,

Operculodinium israelianum,

O. centrocarpum,

O. centrocarpum short processus,

Ataxodinium choane,

Bitectatodinium tepikiense,

Tectatodinium pellitum,

C. Pentapharsodinium dalei,

C. Alexandrium sp.,

C. Scrippsiella trifida,

Pyxidinopsis reticulata,

Nematosphaeropsis labyrinthus

In addition, some of the above taxa have the following characteristics:

Warm-loving sea surface conditions indicators:

O. israelianum, S. pachydermus, P. zoharyi, T. vancampoae and *S. mirabilis*

Seasonal amplitude of sea surface temperature indicators:

B. tepikiense

Supplementary information SI2: The pollen diagrams of cores CS 22 (a) and CS18 (b) for the MIS 5 part of the sequences: percentages re-calculated on a sum without *Pinus* for terrestrial taxa only

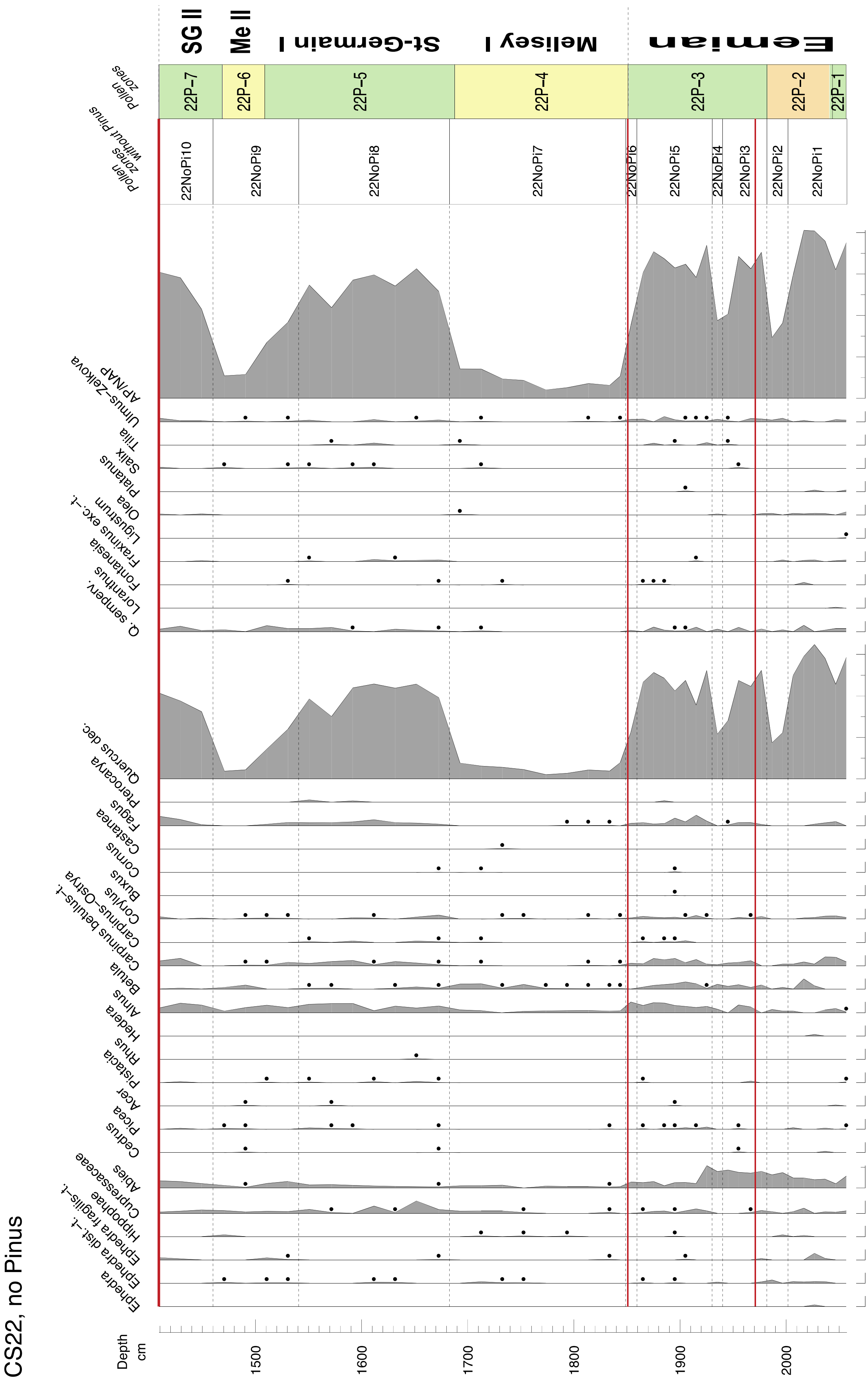

CS22, no Pinus
Depth cm
1500
1600
1700
1800
1900
2000
Ephedra
Ephedra dist.-t.
Ephedra fragilis-t.
Hippophae
Cupressaceae
Abies
Cedrus
Picea
Acer
Pistacia
Rhus
Hedera
Alnus
Betula
Carpinus betulus-t.
Carpinus-Ostrya
Corylus
Buxus
Cornus
Castanea
Fagus
Pterocarya
Quercus dec.
Q. semperv.
Loranthus
Fontanesia
Fraxinus exc.-t.
Ligustrum
Olea
Platanus
Salix
Tilia
Ulmus-Zelkova
AP/NAP
Pollen zones without Pinus
22NoPi10
22NoPi9
22NoPi8
22NoPi7
22NoPi6
22NoPi5
22NoPi4
22NoPi3
22NoPi2
22NoPi1
Pollen zones
22P-7
22P-6
22P-5
22P-4
22P-3
22P-2
22P-1
SG II
Me II
St-Germain I
Melisey I
Eemian

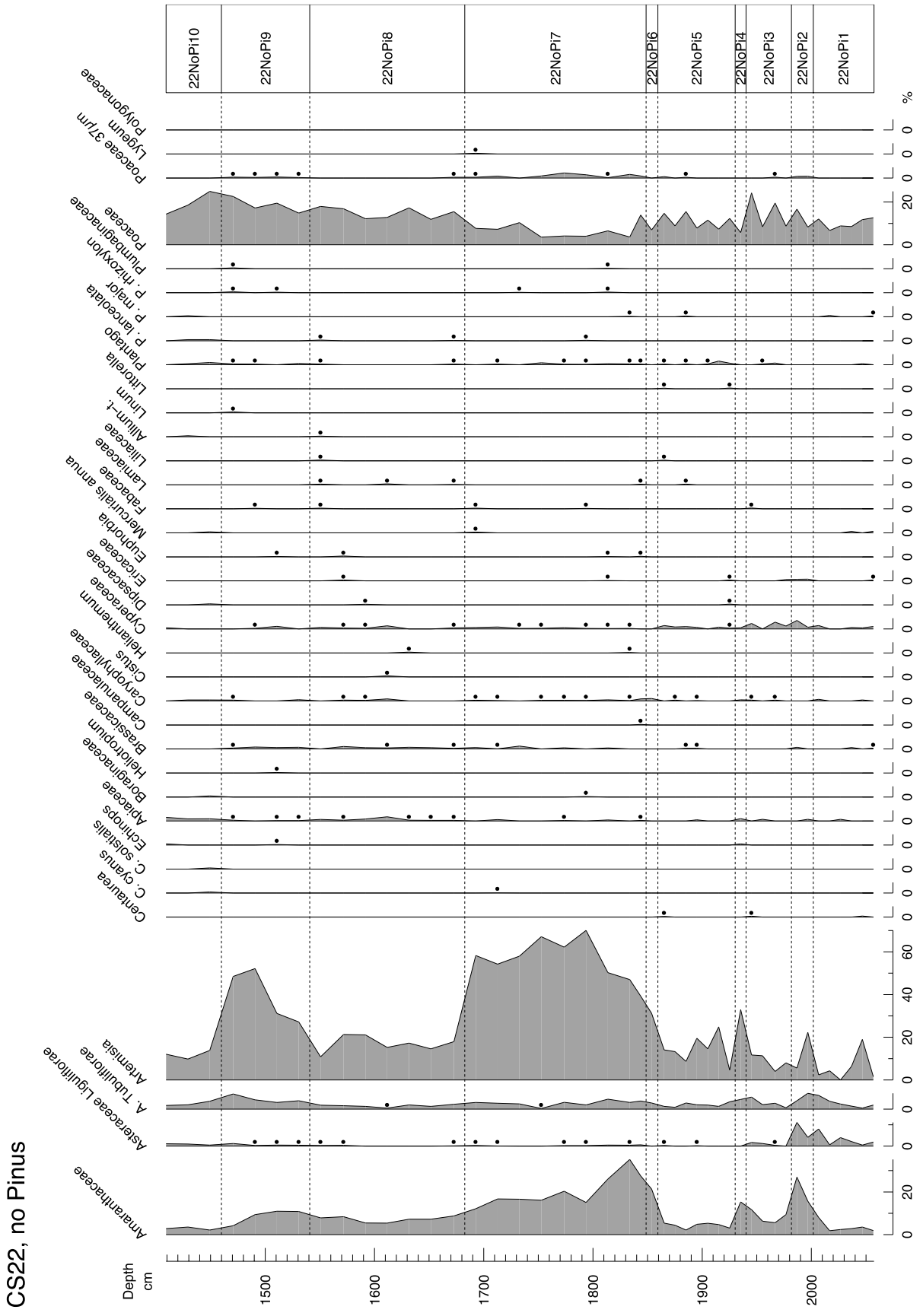
CS22, no Pinus
Depth cm
1500
1600
1700
1800
1900
2000
Amaranthaceae
Asteraceae Liguliflorae
A. Tubuliflorae
Artemisia
Centaurea
C. cyanus
C. solstitialis
Echinops
Apiaceae
Boraginaceae
Helliotropium
Brassicaceae
Campanulaceae
Caryophyllaceae
Cistus
Helianthemum
Cyperaceae
Dipsacaceae
Ericaceae
Euphorbia
Mercurialis annua
Fabaceae
Lamiaceae
Liliaceae
Allium-t.
Linum
Litorella
Plantago
P. lanceolata
P. major
P. rhizoxylon
Plumbaginaceae
Poaceae
Poaceae 37µm
Lygeum
Polygonaceae
22NoPi10
22NoPi9
22NoPi8
22NoPi7
22NoPi6
22NoPi5
22NoPi4
22NoPi3
22NoPi2
22NoPi1
%

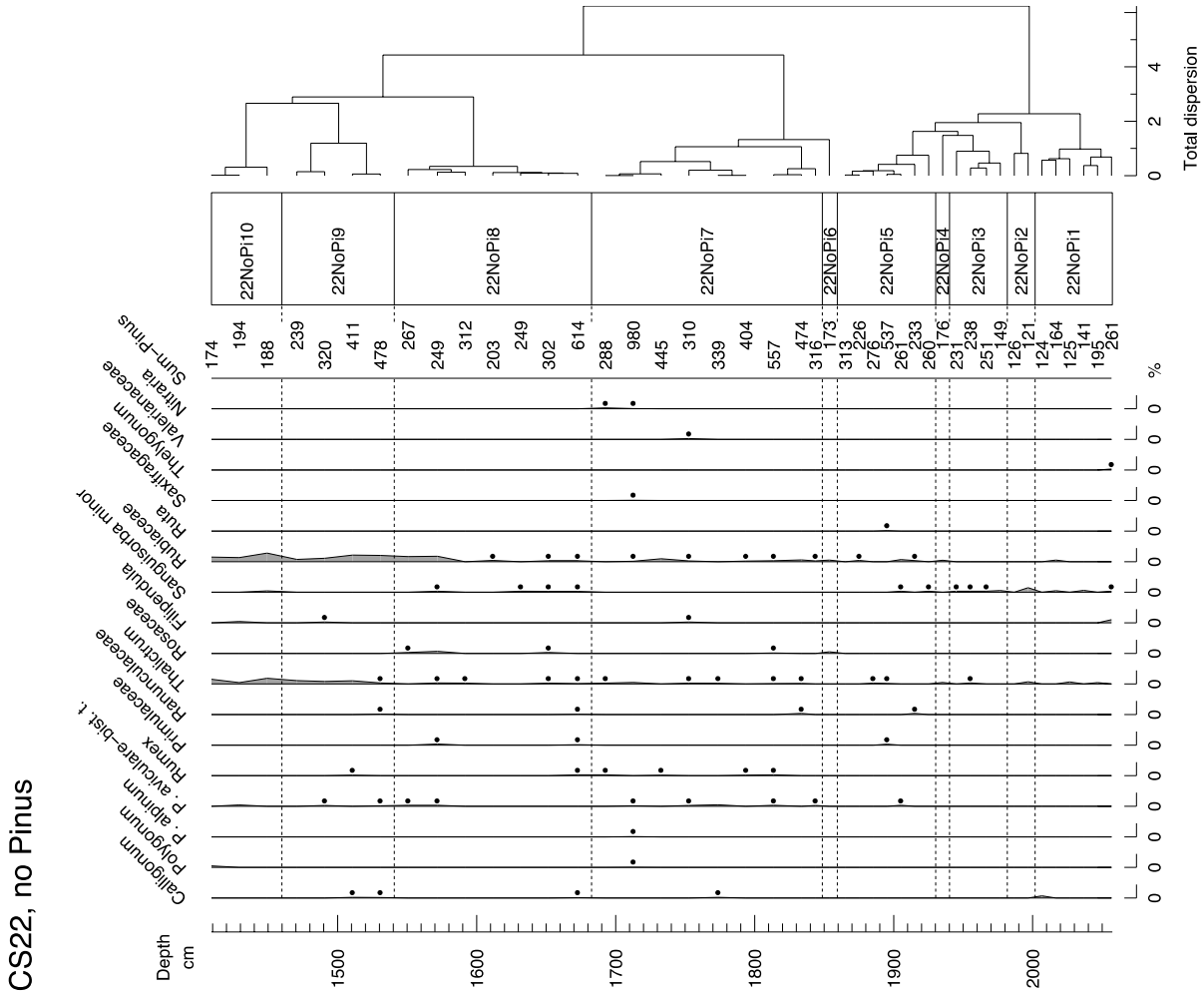
CS22, no Pinus
Depth cm
1500
1600
1700
1800
1900
2000
Total dispersion
0
2
4
22NoPi10
22NoPi9
22NoPi8
22NoPi7
22NoPi6
22NoPi5
22NoPi4
22NoPi3
22NoPi2
22NoPi1
174 194 188
239 320 411 478
267 249 312 203 249 302 614
288 980 445 310 339 404 557 474
316 173
313 226 276 237 261 233 260
176 231 238 251 149
126 121 124 164 125 141 195 261
%
Sum−Pinus
Nitraria
Valerianaceae
Valeriana officinalis
Thelypteridaceae
Saxifragaceae
Rutaceae
Rubus chamaemorus
Sanguisorba officinalis
Filipendula
Rosaceae
Thalictrum
Ranunculaceae
Primulaceae
Rumex
P. aviculare−bist. t.
P. alpinum
P. polygonum
Calliergonum

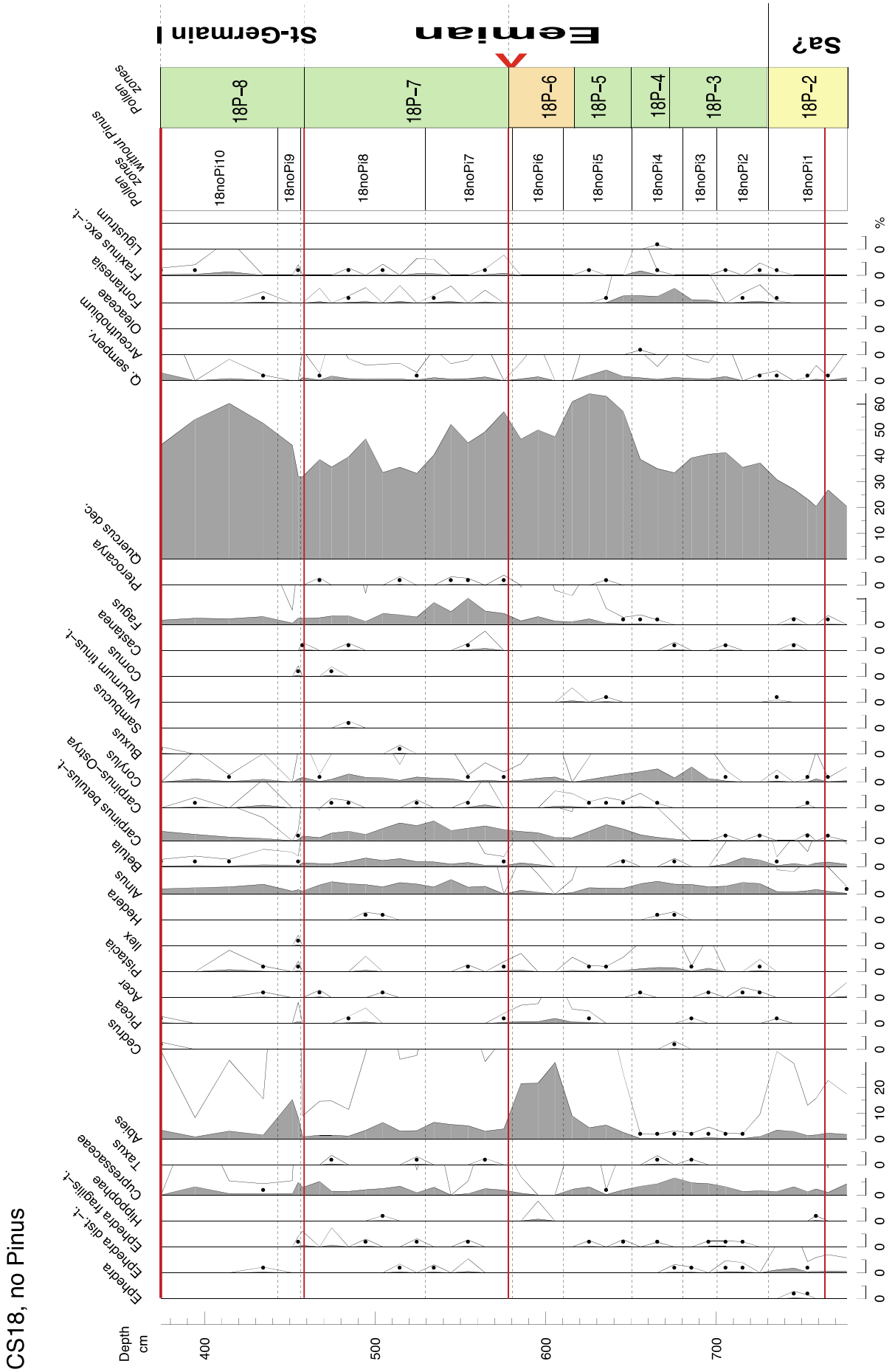
CS18, no Pinus
Depth cm
400
500
600
700
Ephedra
Ephedra dist.-t.
Ephedra fragilis-t.
Hippophae
Cupressaceae
Taxus
Abies
Cedrus
Picea
Acer
Pistacia
Ilex
Hedera
Alnus
Betula
Carpinus betulus-t.
Carpinus-Ostrya
Corylus
Buxus
Sambucus
Viburnum tinus-t.
Cornus
Castanea
Fagus
Pterocarya
Quercus dec.
Q. semperv.
Arceuthobium
Oleaceae
Fontanesia
Fraxinus exc.-t.
Ligustrum
Pollen zones without Pinus
Pollen zones
18noPi10
18noPi9
18noPi8
18noPi7
18noPi6
18noPi5
18noPi4
18noPi3
18noPi2
18noPi1
18P–8
18P–7
18P–6
18P–5
18P–4
18P–3
18P–2
St-Germain I
Eemian
Sa?
%

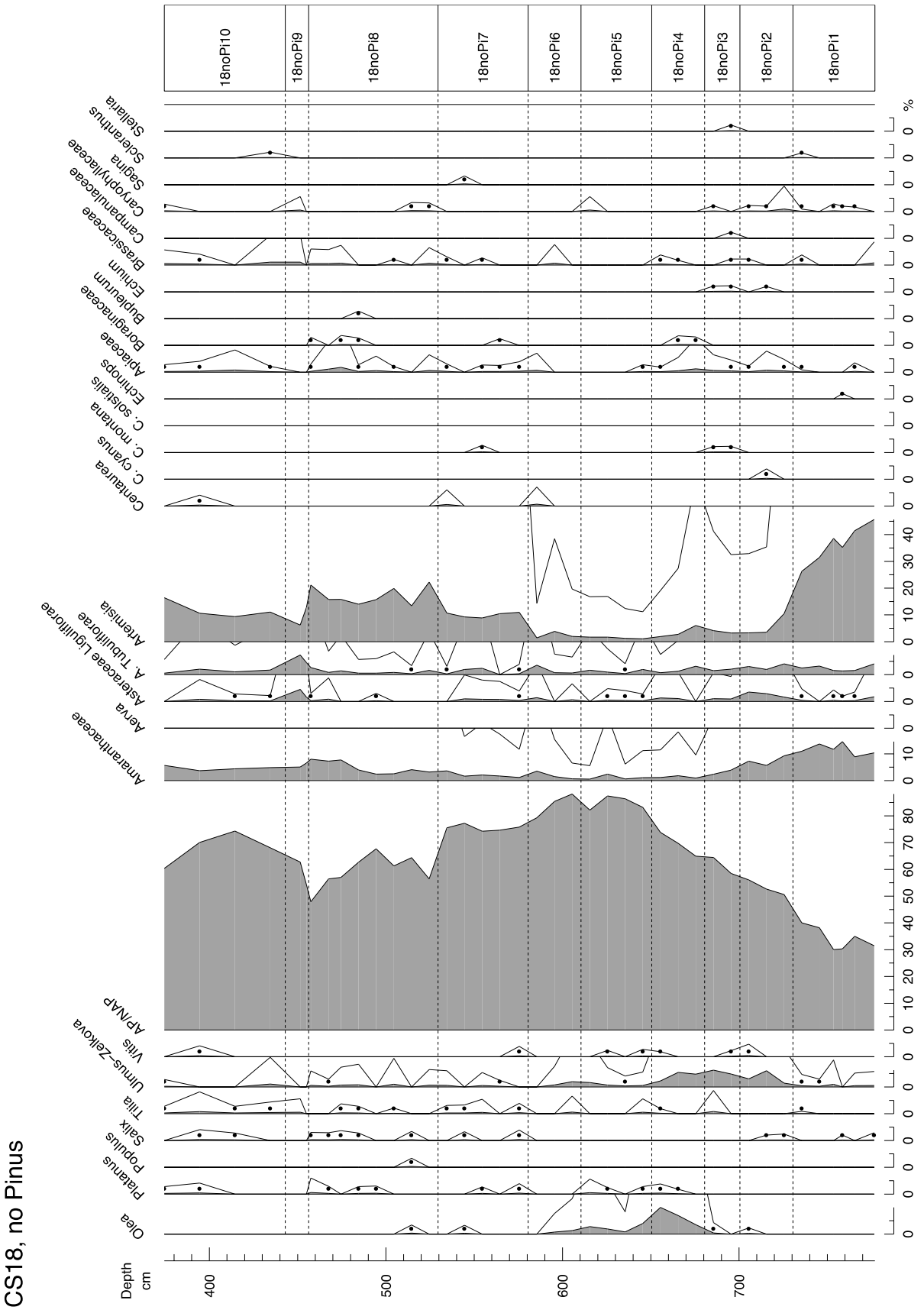
CS18, no Pinus
Depth cm
400
500
600
700
18noPi10
18noPi9
18noPi8
18noPi7
18noPi6
18noPi5
18noPi4
18noPi3
18noPi2
18noPi1
Olea
Platanus
Populus
Salix
Tilia
Ulmus-Zelkova
Vitis
AP/NAP
Amaranthaceae
Artemisia
A. Tubuliflorae Ligulifloriae
Asteraceae
Cerealea
Centaurea
C. cyanus
C. montana
C. solstitialis
Echinops
Apiaceae
Boraginaceae
Bupleurum
Echium
Brassicaceae
Campanulaceae
Caryophyllaceae
Saginа
Scleranthus
Stellaria
%

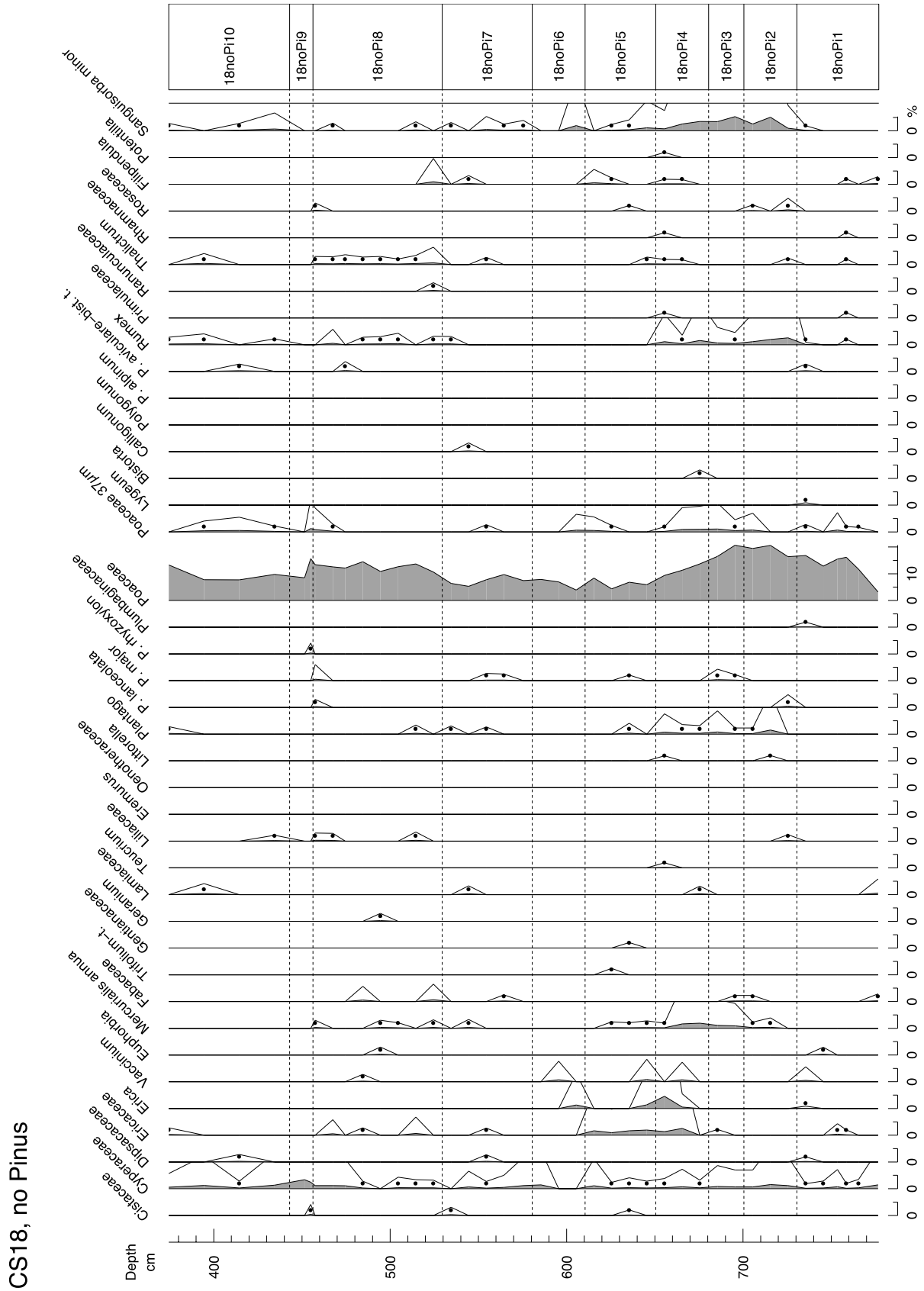
CS18, no Pinus
Depth cm
400
500
600
700
18noPi10
18noPi9
18noPi8
18noPi7
18noPi6
18noPi5
18noPi4
18noPi3
18noPi2
18noPi1
Cistaceae
Cyperaceae
Dipsacaceae
Ericaceae
Erica
Vaccinium
Euphorbia
Mercurialis annua
Fabaceae
Trifolium-t.
Gentianaceae
Geranium
Lamiaceae
Teucrium
Liliaceae
Elemurus
Oenotheraceae
Littorella
Plantago
P. lanceolata
P. major
P. rhyzoxylon
Plumbaginaceae
Poaceae
Poaceae 37µm
Lygeum
Bistorta
Calligonum
Polygonum
P. aviculare-bist.t.
Rumex
Primulaceae
Ranunculaceae
Thalictrum
Rhamnaceae
Rosaceae
Filipendula
Potentilla
Sanguisorba minor
%
0
10

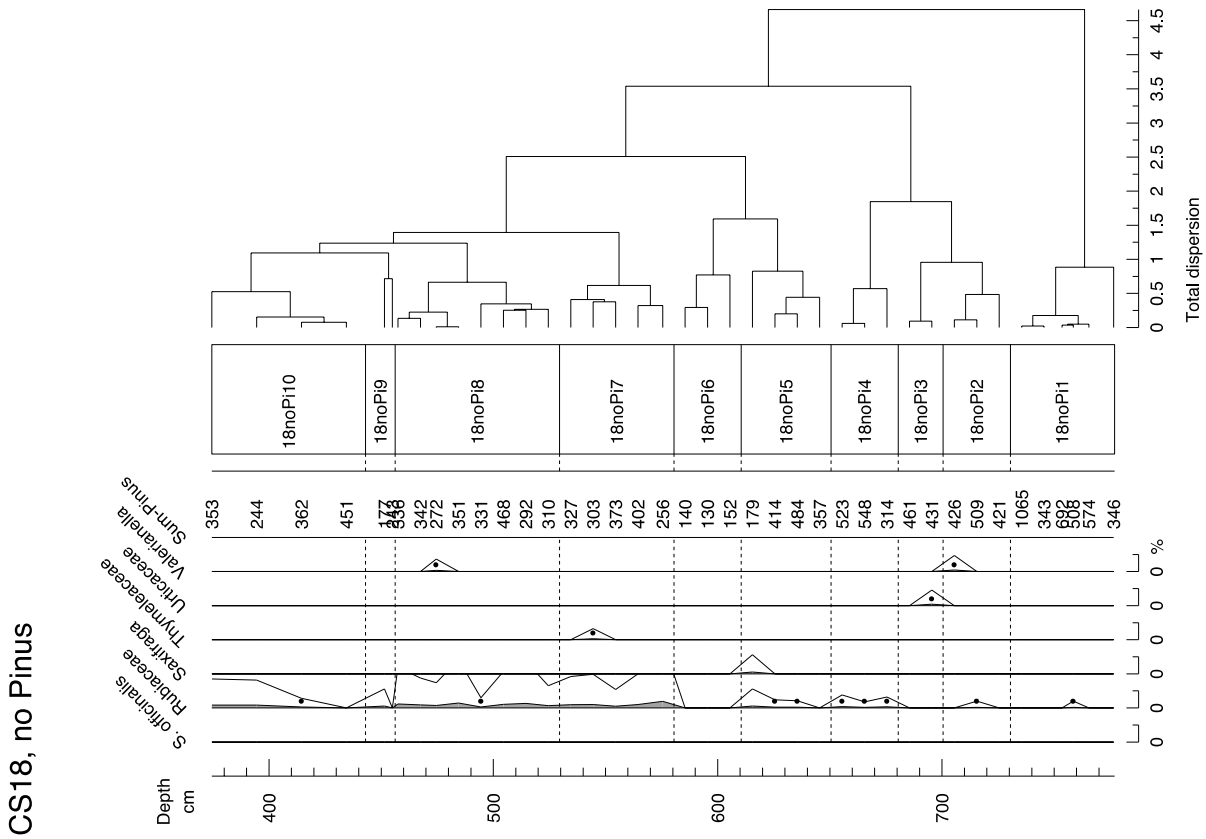
CS18, no Pinus
Total dispersion
0 0.5 1 1.5 2 2.5 3 3.5 4 4.5
18noPi10
18noPi9
18noPi8
18noPi7
18noPi6
18noPi5
18noPi4
18noPi3
18noPi2
18noPi1
353 244 362 451 177 342 272 351 331 468 292 310 327 303 373 402 256 140 130 152 179 414 484 357 523 548 314 461 431 426 509 421 1065 343 574 346
S. officinalis
Rubiaceae
Saxifraga
Thymeleaceae
Urticaceae
Valerianella
Sum-Pinus
0 0 0 0 0 %
Depth cm
400
500
600
700